A Feed-forward Pathway Drives LRRK2 kinase Membrane Recruitment and Activation

Edmundo G. Vides[1,4], Ayan Adhikari[1,4], Claire Y. Chiang[1], Pawel Lis[2,4], Elena Purlyte[2,4], Charles Limouse[1], Justin L. Shumate[1,4], Elena Spínola-Lasso[2,3], Herschel S. Dhekne[1,4], Dario R. Alessi[2,4], and Suzanne R. Pfeffer[1,4]*

[1]Department of Biochemistry, Stanford University School of Medicine

[2]MRC Protein Phosphorylation and Ubiquitylation Unit, University of Dundee

[3]Instituto Universitario de Investigaciones Biomédicas y Sanitarias (IUIBS), Departamento de Bioquímica y Biología Molecular, Fisiología, Genética e Inmunología, Universidad de Las Palmas de Gran Canaria, The Canary Islands, Spain

[4]Aligning Science Across Parkinson's (ASAP) Collaborative Research Network, Chevy Chase, MD

*Corresponding Author

Address:

279 Campus Drive

Stanford, California, USA 94305-5307

E-mail Address: pfeffer@stanford.edu

Abstract

Activating mutations in the Leucine Rich Repeat Kinase 2 (LRRK2) cause Parkinson's disease and previously we showed that activated LRRK2 phosphorylates a subset of Rab GTPases (Steger et al., 2017). Moreover, Golgi-associated Rab29 can recruit LRRK2 to the surface of the Golgi and activate it there for both auto- and Rab substrate phosphorylation. Here we define the precise Rab29 binding region of the LRRK2 Armadillo domain between residues 360-450 and show that this domain, termed "Site #1", can also bind additional LRRK2 substrates, Rab8A and Rab10. Moreover, we identify a distinct, N-terminal, higher affinity interaction interface between LRRK2 phosphorylated Rab8 and Rab10 termed "Site #2", that can retain LRRK2 on membranes in cells to catalyze multiple, subsequent phosphorylation events. Kinase inhibitor washout experiments demonstrate that rapid recovery of kinase activity in cells depends on the ability of LRRK2 to associate with phosphorylated Rab proteins, and phosphorylated Rab8A stimulates LRRK2 phosphorylation of Rab10 in vitro. Reconstitution of purified LRRK2 recruitment onto planar lipid bilayers decorated with Rab10 protein demonstrates cooperative association of only active LRRK2 with phospho-Rab10-containing membrane surfaces. These experiments reveal a feed-forward pathway that provides spatial control and membrane activation of LRRK2 kinase activity.

50 **Introduction**

51 Activating mutations in the Leucine Rich Repeat Kinase 2 (LRRK2) cause inherited Parkinson's
52 disease, and lead to the phosphorylation of a subset of Rab GTPases (Alessi and Sammler,
53 2018), in particular, Rab8A, Rab10, and Rab29 within a conserved residue of the Switch-II
54 effector binding motif. Rab GTPases are master regulators of membrane trafficking and are
55 thought to serve as identity determinants of membrane bound compartments of the secretory
56 and endocytic pathways (Pfeffer, 2017). In their GTP bound forms, Rabs are best known for
57 their roles in linking motor proteins to transport vesicles and facilitating the process of transport
58 vesicle docking.

59

60 Our previous work showed that Rab phosphorylation blocks the ability of Rab proteins to be
61 activated by their cognate guanine nucleotide exchange factors or to bind to the GDI proteins
62 that recycle GDP-bearing Rabs from target membranes to their membranes of origin (Steger et
63 al., 2016; 2017). Moreover, phosphorylation of Rab8A and Rab10 blocks their ability to bind
64 known effector proteins and enhances binding to a novel set of effectors that includes RILPL1,
65 RILPL2, JIP3, JIP4 and MyoVa proteins (Steger et al., 2017; Waschbüsch et al., 2020; Dhekne
66 et al., 2021). Thus, Rab phosphorylation flips a switch on Rab effector selectivity that can drive
67 dominant physiological changes, including blocking primary cilia formation (Steger et al., 2017;
68 Dhekne et al., 2018; Sobu et al., 2021; Khan et al., 2021) and autophagosome motility in axons
69 (Boecker et al., 2021).

70

71 Most LRRK2 is found in the cell cytosol where it appears to be inactive (Biskup et al., 2006;
72 Berger et al., 2010; Purlyte et al., 2018). Recent structural analysis of the catalytic, C-terminal
73 half of LRRK2 (Deniston et al., 2021) and full length human LRRK2 protein yielded structures of
74 both monomeric and dimeric, inactive states (Myasnikov et al., 2021). Several groups have
75 reported that active LRRK2 is a dimer (Greggio et al., 2008; Klein et al., 2009; Sen et al., 2009;

Berger et al, 2010; Civiero et al., 2012; Guaitoli et al, 2016), and higher order forms were detected on membranes upon crosslinking (Berger et al., 2010; Schapansky et al., 2014) and upon Rab29 binding (Zhu et al., 2022). Thus, LRRK2 membrane association is associated with kinase activation, however the molecular basis for this activation is not yet known.

Exogenously expressed, Golgi-localized Rab29 protein can recruit LRRK2 onto membranes and activate it there for both auto- and Rab substrate phosphorylation (Kuwahara et al., 2016; Liu et al., 2018; Purlyte et al., 2018; Madero-Pérez et al., 2018). Indeed, even Rab29 artificially anchored on mitochondria can activate LRRK2 and drive its membrane recruitment (Gomez et al., 2019). McGrath et al. (2021) implicated LRRK2 residues 386-392 as being important for the interaction of Rab29/32/38 family members with the LRRK2 kinase Armadillo domain. However, the LRRK2 Armadillo domain is located at some distance from the kinase domain, at least in the current structure models for LRRK2 protein (Myasnikov et al., 2021). Thus, how Rab29 binding might activate LRRK2 kinase activity is not at all clear. In addition, because Rab29 is not needed for LRRK2 action on Rab8A or Rab10 proteins (Kalogeropulou et al., 2020), other pathways for LRRK2 activation must exist.

In this study, we define a specific patch (“Site #1”) of the LRRK2 Armadillo domain that binds to Rab8A, Rab10 and Rab29 protein with affinities similar to those reported previously (McGrath et al., 2021). More importantly, we identify a distinct region of LRRK2 Armadillo domain (“Site #2”) that binds specifically to LRRK2-*phosphorylated* Rab8A and Rab10 proteins, to establish a feed forward activation mechanism for membrane-associated LRRK2 kinase.

102 **Results**

103 **Rab29 binds to the C-terminal portion of the LRRK2 Armadillo domain**

104 McGrath et al. (2021) showed that the LRRK2 Armadillo domain residues 1-552 contain a
105 binding site that interacts specifically with purified Rab29, 32 and 38 in vitro with affinities of 2.7,
106 1.2 and 1.2-2.4μM, respectively. We used microscale thermophoresis to determine the affinity
107 of other Rab GTPase substrates with this portion of LRRK2 kinase. For these experiments,
108 portions of the LRRK2 Armadillo domain were fluorescently labeled and incubated with Rab
109 GTPases in the presence of Mg^{2+}-GTP. Figure 1 shows binding curves for Rab29 with full
110 length Armadillo domain (residues 1-552, panel A), as well as sub-fragments composed of
111 LRRK2 residues 1-159 (Fig. 1C) or 350-550 (Fig. 1D). Rab29 showed specific binding to the full
112 length 1-552 Armadillo fragment with a K_D of 1.6μM (Fig. 1A), comparable to that reported
113 previously using other methods (McGrath et al., 2021). Under these conditions, the non-LRRK2
114 substrate Rab7 protein failed to bind to the Armadillo 1-552 fragment (Fig. 1B). No Rab29
115 binding was detected to a fragment representing the N-terminal 1-159 LRRK2 residues (binding
116 >29μM; Fig. 1C); essentially full binding was observed with a fragment encompassing residues
117 350-550 (K_D = 1.6μM; Fig. 1D). Thus, Rab29 binds to the C-terminal portion of LRRK2's
118 Armadillo domain at a site that we will refer to as Site #1.

119

120 **Rab8A and Rab10 bind to the LRRK2 Armadillo domain**

121 Similar experiments were carried out with Rab8A and Rab10, the most prominent LRRK2
122 substrates (Steger et al., 2017). Rab8A bound full length Armadillo domain with a K_D of 2.9μM
123 (Fig. 2A), showed weaker interaction with the LRRK2 1-159 fragment (K_D ~ 6.7μM; Fig. 2B), and
124 good binding to the 350-550 fragment (K_D = 2.3μM; Fig. 2C). These data indicate that Rab8A
125 may bind to the same site as Rab29. Like Rab8A, Rab10 bound to full length Armadillo 1-552
126 with a K_D of 2.4μM (Fig. 2D); weaker binding was detected for 1-159 and 350-550 fragments,
127 yielding K_Ds of 5.1μM in both cases (Fig. 2E,F). Thus, in addition to Rab32, 38 and 29, Rabs

128 8A and 10 can bind to LRRK2 residues 350-550. Note that Rab32 and Rab38 are not
129 substrates of LRRK2 kinase as they lack a phosphorylatable Ser/Thr residue in the Switch-II
130 motif (Steger et al., 2016; 2107); they show extremely narrow tissue-specific expression but are
131 related to Rab29 protein.
132
133 **Residues critical for Rab GTPase binding to LRRK2 residues 350-550, Site #1**
134 Previous work implicated LRRK2 residues 386–392 in contributing to a Rab29/32/38 binding
135 interface (McGrath et al., 2021). We used a microscopy-based assay to identify any portions of
136 the first 1000 residues of LRRK2 that would relocalize to the Golgi upon co-expression with
137 Golgi localized, HA-Rab29 protein (Fig. 3-Fig. Suppl. 1). Twenty two constructs were
138 transfected into cells and their localization scored visually. The smallest fragment of LRRK2
139 that interacted with HA-tagged Rab29 in HeLa cells, thereby co-localizing at the Golgi complex,
140 encompassed LRRK2 residues 350-550.
141
142 We next deployed AlphaFold docking (Jumper et al., 2021) using ColabFold (Mirdita et al.,
143 2022) and the AlphaFold2_advanced.ipynb notebook with the default settings to model the
144 interaction of Rab29 with the LRRK2 350-550 fragment (Fig. 3A and Fig. 3-Fig. Suppl. 2).
145 Residues highlighted in red show key contacts between LRRK2 and Rab29 and will be shown
146 below to be essential for detection of this interaction in cells. This modelled structure of Site #1
147 is extremely similar to that of the recently reported experimental cryo-EM structure of Rab29
148 complexed full length LRRK2 (Zhu et al 2022).
149
150 Three metrics were used to evaluate the importance of individual residues to contribute to
151 Rab29 interaction. First, we tested the impact of mutations on the ability of full length LRRK2 to
152 co-localize with HA-Rab29 at the Golgi in HeLa cells (Fig. 3B and Fig.3 – Fig. Suppl. 3); we also
153 tested the ability of exogenously expressed Rab29 to stimulate activity of the same point

154 mutants in the background of either wild type LRRK2 (Fig. 3C, Fig. 3–Fig. Suppl. 4A) or
155 pathogenic R1441G LRRK2 (Fig. 3D, Fig 3.--Fig. Suppl. 4B). This work identified 4 key
156 mutations of highly conserved residues (R361E, R399E, L403A and K439E) that blocked both
157 the co-localization of LRRK2 and Rab29 in HeLa cells (Fig. 3B, red) as well as activation of
158 LRRK2 upon overexpression of Rab29 in HEK293 cells (Fig. 3C, red). In experiments
159 undertaken with pathogenic R1441G LRRK2 that is more potently activated by Rab29, the
160 K439E LRRK2 mutation completely blocked LRRK2 kinase activation; R399E showed weak
161 activation (Fig. 3D and Fig. 3--Fig. Suppl. 4B). Some of the other mutants blocked co-
162 localization with Rab29 in HeLa cells without completely suppressing LRRK2 activation
163 following overexpression of Rab29. We therefore recommend using the Site#1 K439E LRRK2
164 mutation to block Rab29 interaction and activation in future work (asterisks in Figs. 3B,C) as it
165 shows the lowest amount of Rab29 activation with pathogenic R1441G LRRK2. Altogether,
166 these data highlight the importance of a surface that is comprised of LRRK2 residues Arg361,
167 Arg399, Leu403, Lys439 in binding Rab GTPases (Site #1) (Fig. 3A and Fig. 3 -Fig. Suppl. 2).
168 Analysis of Rab8A interaction with the LRRK2 350-550 fragment using AlphaFold within
169 Chimera X 1.4 confirmed the importance of the same LRRK2 residues for Rab8A interaction in
170 silico (Figure 3-Fig. Supplement 2C).
171
172 **PhosphoRab binding to LRRK2, Site #2**
173 To understand the consequences of LRRK2-mediated Rab GTPase phosphorylation, it is
174 important to identify specific binding partners of phosphorylated Rab proteins, and to study the
175 consequences of such binding events. We recently established a facile method that enables us
176 to monitor phosphoRab binding to proteins of interest in conjunction with microscale
177 thermophoresis binding assays. Briefly, Rab proteins are phosphorylated >90% in vitro by
178 MST3 kinase (Dhekne et al., 2021; Vides and Pfeffer, 2021) that phosphorylates Rab proteins at
179 the same position as LRRK2 kinase (Vieweg et al., 2020). Recombinant MST3 is much easier

180 to purify in large amounts for biochemical experiments than LRRK2. We used this assay to
181 monitor the possible interaction of phosphorylated LRRK2 substrates to the LRRK2 Armadillo
182 domain and were delighted to discover that pRab8A and pRab10 proteins bind with high affinity
183 to a site distinct from that used by non-phosphorylated Rab proteins that we term site #2.
184
185 As shown in Fig. 4, phosphoRab8A and phosphoRab10 bound with K_Ds of ~900nM and 1μM to
186 the full Armadillo domain 1-552 fragment, respectively (Figs. 4A, D); this binding reflected
187 interaction with N-terminal LRRK2 residues 1-159, as this fragment was sufficient to yield
188 essentially the same K_Ds of 1μM and 700 nM, respectively for phosphoRab8A and
189 phosphoRab10 proteins (Figs. 4B, E). Furthermore, no binding was detected for
190 phosphoRab8A or phosphoRab10 with LRRK2 residues 350-550 (Figs. 4C, F). These data
191 demonstrate that Rab8A and Rab10 GTPases, phosphorylated at the same residues modified
192 by LRRK2 kinase bind very tightly to the LRRK2 N-terminus but no longer interact with the 350-
193 550 region that interacts with dephosphorylated Rab proteins.
194
195 Note that non-phosphorylated Rab8A and Rab10 also bound to the Site #2-containing fragment
196 1-159 with relatively weak affinities of 5 or 6μM (Fig. 2B,E; Table 1). Interestingly, AlphaFold in
197 Chimera X predicts that the 1-159 fragment contains a potential, non-phosphoRab binding site
198 that is occluded in a longer fragment (1-400), and thus also in full length LRRK2. Moreover, as
199 discussed below, these K_D values may be higher than the concentrations of these Rab
200 GTPases in cells, thus it seems unlikely that non-phosphoRabs interact with Site #2 under
201 normal physiological conditions. We conclude that phosphoRab binding is the predominant
202 interaction between LRRK2 1-159 and Rab GTPases.
203
204 Electrostatic analysis of a model of the LRRK2 Armadillo domain revealed that the absolute N-
205 terminus of LRRK2 contains a patch of basic amino acids (highlighted in blue) that may

206 comprise a phosphoRab interaction interface (Fig. 5A) (Jurus et al., 2018; Pettersen et al.,
207 2004). Such modeling led us to test the role of lysine residues at positions 17 and 18 in
208 mediating LRRK2 interaction. Mutation of either lysine 17 or 18 abolished phosphoRab10
209 binding to LRRK2 Armadillo domain, with binding decreased to >20μM upon single mutation at
210 either site (Fig. 5C, D). When the conservation score of these residues is analyzed using the
211 Consurf server (Ashkenazy et al., 2016) K17 and K18 have a score or 2 and 8 respectively (9 is
212 the maximum score), indicating that K18 is highly conserved and plays an especially important
213 role. These experiments define a second, Rab binding site #2 that is specific for
214 phosphorylated Rab proteins (Fig. 5B).
215
216 To determine the significance of the phosphoRab binding site in relation to LRRK2 membrane
217 recruitment in cells, we generated full length FLAG-LRRK2 protein containing point mutations at
218 both lysines 17 and 18 and investigated its cellular localization upon expression in HeLa cells
219 (Fig. 6). To improve our ability to detect membrane associated LRRK2 distribution, cells grown
220 on collagen coated coverslips were dipped in liquid nitrogen and then thawed in a physiological,
221 glutamate-containing buffer to crack open the plasma membrane and release cytosolic proteins
222 prior to fixation (Seaman et al., 2004; Purlyte et al., 2018). Under these conditions, LRRK2 co-
223 localizes with phosphorylated Rab proteins (Purlyte et al., 2018; Sobu et al., 2021).
224
225 As expected, PhosphoRab10 was detected as a bright spot adjacent to the mother centriole in
226 HeLa cells (Fig. 6A), and the co-expressed, R1441G pathogenic mutant LRRK2 protein showed
227 good co-localization with phosphoRab10 protein (Figs. 6A,C), as we have reported previously
228 (Purlyte et al., 2018; Sobu et al., 2021). In contrast, although exogenously expressed, R1441G
229 LRRK2 bearing K17/18/A mutations still generated a perinuclear, phosphoRab10-containing
230 structure, LRRK2 displayed much less co-localization with the phosphoRab proteins or with
231 membranes overall (Figs. 6B,C). These experiments show that K17 and K18 are important for

232 exogenous LRRK2 membrane association with a pool of highly phosphorylated Rab10 protein.
233 The importance of LRRK2's N-terminal lysine residues also suggests that caution may be in
234 order when evaluating membrane interactions of LRRK2 tagged N-terminally with larger tags
235 such as GFP that may hinder access to K17/K18.
236
237 **PhosphoRab-LRRK2 interaction increases rates of kinase recovery**
238 We next explored the relevance of phosphoRab binding to LRRK2's N-terminus in relation to the
239 overall kinetics of Rab phosphorylation in cells. LRRK2-mediated Rab GTPase phosphorylation
240 is a highly dynamic process that is counteracted by the action of PPM1H phosphatase
241 (Berndsen et al., 2019); at steady state, only a small fraction of total Rab proteins are LRRK2-
242 phosphorylated (Ito et al., 2016). The initial rate of kinase activity can be determined by
243 monitoring the phosphorylation of Rab10 protein after washout of the LRRK2 inhibitor, MLi-2 (Ito
244 et al., 2016; Kalogeropulou, 2020).
245
246 When HeLa cells were treated with 200nM MLi-2 for 1hr and then washed with culture medium,
247 Rab10 was efficiently re-phosphorylated by exogenous, FLAG-tagged, R1441G LRRK2 protein
248 over the 2h time course evaluated (Fig. 7A, E). In contrast, cells expressing FLAG-R1441G
249 LRRK2 bearing K17/18A mutations showed comparable total phosphoRab10 levels to begin
250 with, but significantly slower re-phosphorylation (Fig 7B, E). Similar results were obtained in
251 experiments comparing the re-activation of FLAG-tagged, wild type LRRK2 (Fig. 7C,F) with that
252 of LRRK2 K17/18A (Fig. 7D,F). As reported previously (Ito et al., 2016), wild type LRRK2
253 recovery was more efficient than that of R1441G LRRK2. In summary, these experiments
254 demonstrate that K17/K18 residues are important for efficient reactivation of LRRK2 after MLI-2
255 washout, consistent with their role in anchoring LRRK2 at sites adjacent to phosphorylation
256 substrates.
257

258 **Cooperative LRRK2 membrane recruitment on Rab-decorated planar lipid bilayers**

259 Binding of phosphoRabs to Site #2 at the N-terminus of LRRK2 (Fig. 5B) would set up a feed-
260 forward process whereby the product of an initial phosphorylation reaction would enhance
261 subsequent Rab GTPase phosphorylation by holding the enzyme on the surface of membranes
262 that contain relevant Rab GTPase substrates. To visualize the membrane association process
263 directly, we established a planar lipid bilayer system that would enable us to monitor the
264 interaction of fluorescently labeled, purified, full length LRRK2 kinase with membrane anchored
265 Rab10 substrate (Adhikari et al., 2022). For this purpose, bilayers were formed on the surface
266 of glass bottom chambers comprised of phospholipids of a composition similar to that found in
267 the Golgi (65% DOPC, 29% DOPS, 1% PI(4)P (Thomas and Fromme, 2016), mixed with 0.1%
268 of the lipophilic tracer DiD dye and 5% DOGS-NTA [Ni^2] to to enable anchoring of C-terminally
269 His-GFP-tagged Rab10 protein. Binding of fluorescently labeled, hyperactive R1441G LRRK2
270 was then visualized in real time using total internal reflection (TIRF) light microscopy. Reactions
271 were carried out in the presence of ATP, GTP and an ATP regenerating system to provide
272 physiological conditions for the full length LRRK2 enzyme. Note that we routinely utilize
273 R1441G LRRK2 because it is a highly active kinase in cells, although in vitro, R1441G LRRK2
274 displays the same level of Rab kinase activity as wild type LRRK2 (cf. Steger et al., 2017).
275

276 As shown in Figure 8A (red dots), fluorescent R1441G LRRK2 bound efficiently to lipid bilayers,
277 only in the presence of pre-anchored Rab10 protein (compare with purple dots in 8B) and not
278 when Rab11 protein was instead employed (Fig. 8B, green dots; movies 1-3). Importantly,
279 almost no binding was observed with kinase inactive D2017A LRRK2 (Fig. 8A yellow dots,
280 movie 4) (Steger et al., 2016). This indicates that at least Rab10 GTPase binding to Site #1
281 residues 361-451 results in a low affinity interaction that is not sufficient to retain this inactive
282 LRRK2 protein on the bilayer under these conditions (7nM LRRK2, 2.5 μM Rab10). Reactions
283 containing the Type I MLi-2 inhibitor showed aggregation of the fluorescent LRRK2 protein, as

284 has been seen in cells. Incubations containing the Type 2 inhibitor, GZD-824 (Tasegian et al.,
285 2021) showed weak binding, consistent with a requirement for phosphoRab10 generation to
286 support LRRK2 binding to Site #2's K17 and K18; however, under these conditions, LRRK2 was
287 not monodisperse and could not be analyzed further. Importantly, R1441G LRRK2 mutated at
288 lysines 17 and 18 bound to a lower extent than R1441G LRRK2 (Fig. 8A, blue dots; movie 5),
289 confirming their important role in binding to phosphorylated Rab8A and Rab10. It is noteworthy
290 that the K17/K18 mutant protein showed higher binding than the D2017A mutant, suggesting
291 that a non-phosphoRab binding site may be more accessible for binding in an active versus
292 inactive LRRK2 protein conformation.
293
294 Analysis of the kinetics of LRRK2 binding as a function of Rab protein concentration showed
295 clear, cooperative membrane association of R1441G LRRK2, consistent with a feed-forward
296 mechanism, as predicted from the in vitro Rab binding data (Fig. 8C). A nonlinear regression fit
297 of the data indicated a Hill coefficient of 2.7, consistent with a positive, cooperative
298 phenomenon. In summary, these data demonstrate that LRRK2 kinase is recruited to
299 membranes and then held there by phosphorylated Rabs to increase subsequent Rab GTPase
300 phosphorylation as part of a cooperative, feed-forward pathway.
301
302 LRRK2 is difficult to dye-label mono-molecularly, as the N-terminus is engaged in phosphoRab
303 binding and the C-terminus is critical for activity. Nevertheless, analysis of the distribution of
304 single molecule fluorescence intensity of our CF633-labeled LRRK2 preparation revealed a
305 sharp peak, whether the preparation was evaluated immediately upon binding to Rab10 on
306 bilayers (Figure 8–Figure Supplement 1A, B, D) or when spotted onto poly-lysine coated glass
307 (Figure 8–Figure Supplement 1B, far right column). Panels A and B show the intensity at time t
308 for large numbers of fluorescent molecules, either over 500 seconds (A) or 30 seconds (B). The
309 intensity shift over time (panels A,B) may imply that the molecules slowly dimerize with a half

310 time of 100-200 seconds, but additional work would be needed to confirm this. Continuous
311 traces of the 30 longest lived spots showed that for some events this increase occurs even
312 more quickly (1C). The fluorescent molecules remain on the bilayers for a significant period of
313 time (panel E); moreover, when the molecules first bind to the surface, the single peak
314 distribution of intensity does not change, irrespective of the time during the experiment that it
315 actually binds (panel E). This gives us confidence that any changes observed were not
316 occurring in solution and require Rab engagement. Note that we detect a minor species at
317 $\log_2$=2.5 that constitutes between 2 and 6% of the molecules (panels D, F); this may represent
318 dual labeled proteins and/or rare tetrameric complexes.
319
320 To confirm that LRRK2 Armadillo domain can bind both non-phosphorylated and
321 phosphorylated Rabs simultaneously, GST-Rab8A was immobilized on glutathione agarose and
322 Armadillo domain (1-552) protein pre-bound. Purified, phosphoRab10 was then added, and
323 immunoblotting showed that phosphoRab10 bound to the beads only in the presence of Rab8A-
324 anchored, Armadillo fragment (Figure 8 – Figure Supplement 2). Binding at both sites #1 and
325 #2 is predicted to increase avidity of LRRK2 membrane association, consistent with our
326 membrane recruitment data.
327
328 **PhosphoRab8 activates LRRK2 phosphorylation of Rab10 protein**
329 The data presented thus far are consistent with apparent activation of LRRK2 by cooperative
330 recruitment of the kinase to membrane microdomains enriched in Rab protein substrates. It
331 was formally possible, however, that phosphoRab binding actually activates the kinase itself.
332 To test this, we monitored the generation of phosphoRab10 using a highly specific monoclonal
333 antibody in conjunction with immunoblotting. Rab10 protein was then phosphorylated by
334 purified, full length LRRK2 kinase in vitro, with and without addition of pre-phosphorylated
335 Rab8A protein. As shown in Figure 9 (A, C), the presence of stoichimetrically phosphorylated

336 Rab8A (Dhekne et al., 2021) stimulated the rate of in vitro Rab10 phosphorylation by
337 approximately 4 fold. Importantly, the ability of phosphoRab8A to stimulate LRRK2-mediated
338 Rab10 phosphorylation required LRRK2's K18 that is needed for phosphoRab binding (Fig. 9 B,
339 D). We speculate that phosphoRab binding to the absolute N-terminus influences LRRK2's
340 higher order structure to stimulate kinase activity.
341
342 **Discussion**
343 LRRK2 is ~90% cytosolic (Purlyte et al., 2019), and little was known about why membrane-
344 associated LRRK2 appears to be much more active than the cytosolic pool of kinase. We have
345 confirmed here that LRRK2 kinase relies upon substrate Rab GTPases to achieve membrane
346 association, and revealed that LRRK2 utilizes two distinct Rab binding sites within its N-terminal
347 Armadillo domain for this purpose. Site #1 (Fig. 5B) binds multiple, non-phosphorylated Rab
348 substrates including Rab8A, Rab10 and Rab29, as well as the highly tissue specific- and non-
349 substrate, Rab29-related, Rab32 and Rab38 proteins (Waschbüsch et al., 2014; McGrath et al.,
350 2021). The second site (#2) is located at LRRK2's absolute N-terminus, at a significant distance
351 from the kinase active site; this site shows strong preference for phosphorylated Rab8A and
352 Rab10 proteins. Our data show that both sites can be occupied simultaneously.
353
354 Figure 10 shows our current model for LRRK2 membrane recruitment. LRRK2 will interact
355 reversibly with any one of the subset of Rab proteins that can bind to site #1. Rab29 shows the
356 highest affinity for this site, but Rab8A can also bind with physiologically relevant affinity and is
357 much more abundant in cells. Rab GTPases cluster in microdomains on distinct membrane
358 surfaces (Pfeffer, 2017; Sönnichsen et al., 2000; DeRenzis et al., 2002; Barbero et al., 2002),
359 thus this initial LRRK2 membrane association will bring the kinase in contact with other copies
360 of the same substrate Rab proteins for phosphorylation. After an initial phosphorylation event,
361 LRRK2 will then be held in place by bivalent association with one phosphorylated and one non-

362 phosphorylated Rab protein. By binding to the kinase reaction product, LRRK2 enhances its
363 effective, local activity by increasing the probability with which it will encounter another substrate
364 Rab protein.
365
366 Despite relatively similar affinities for their respective Rab binding partners, the phosphoRab-
367 specific site appears to drive stable LRRK2 membrane association, as mutation of two key
368 lysine residues strongly impacts co-localization of LRRK2 protein with phosphoRabs in cells. In
369 addition, kinase activity leads to a much higher degree of LRRK2 association with planar lipid
370 bilayers, despite the presence of binding Site #1 for non-phosphorylated-Rabs. Finally,
371 K17/K18A LRRK2 that cannot bind to phosphorylated Rab proteins showed lower bilayer
372 association in comparison with native LRRK2, confirming the importance of this interaction.
373 LRRK2 phosphorylation of Rab GTPases is therefore required to form a new, additional
374 interaction interface that greatly enhances the overall avidity of LRRK2 membrane association.
375
376 We also discovered that phosphoRab8A stimulates LRRK2 kinase action on Rab10 protein. We
377 were not able to test the reverse scenario as the phosphoRab8A antibody is not adequately
378 specific and cross-reacts with phosphoRab10 protein. Nevertheless, it seems very likely that
379 phosphoRab10 will also activate LRRK2 for other substrate phosphorylation events. The most
380 likely explanation is that phosphoRab binding to the LRRK2 N-terminus encourages an overall
381 enzyme architecture that favors the active conformation. LRRK2 assumes multiple oligomeric
382 states, and phosphoRab engagement and/or dual Rab engagement of the Armadillo domain
383 likely influences the overall architecture of the enzyme.
384
385 It is important to note that quantitative mass spectrometry indicates that Rab10 is present at
386 ~600 times the copy number as LRRK2 in MEF cells and brain tissue
387 (https://copica.proteo.info/#/copybrowse). Thus, if Rab10 is assumed to exist in cells at ~2-5μM

388 (Itzhak et al., 2016), LRRK2 will be present overall at about 3-8nM. These are very close to the
389 concentrations used in our in vitro reconstitution experiments. Future experiments will be
390 needed to elucidate the precise molecular state of LRRK2 upon engagement with Rab GTPases
391 at sites #1 and #2.
392
393 Nichols et al. (2007) reported a single family with two affected siblings harboring LRRK2 E10K
394 mutations. These patients presented with classic Parkinson's disease symptoms at age 57
395 including bradykinesia, muscular rigidity, postural instability, and resting tremor. Compared with
396 46 G2019S LRRK2 patients in that study whose disease onset was on average, 63.5 years, the
397 two siblings had a more severely disabling disease, as indicated by a higher Hoehn and Yahr
398 assessment score (4 versus 2.5, where 5 represents confinement to bed or wheelchair unless
399 aided). Our study provides a molecular explanation for how a mutation located far from the
400 kinase or ROC-COR domains may cause Parkinson's disease. We predict that the E10K
401 mutation increases LRRK2 phosphoRab binding and membrane association and may display an
402 even higher apparent activity than the most common pathogenic G2019S mutation. This
403 distinction would need to be evaluated under conditions of MLi-2 washout, as exogenous
404 expression would mask this subtle mechanistic feature.
405
406 The ability of multiple Rab binding sites to anchor LRRK2 on membranes will make the kinase
407 appear more active than the pool of cytosolic LRRK2 protein. Rab binding may also increase
408 access of LRRK2 to other kinases that stabilize it in a more active conformation. Anchoring
409 LRRK2's N-terminus may also influence autophosphorylation, which could also drive LRRK2
410 towards a more catalytically active conformation. Future structural studies of membrane
411 anchored LRRK2 will provide important, additional information related to all of these
412 possibilities.
413

414

KEY RESOURCES TABLE				
Reagent type (species) or resource	**Designation**	**Source or reference**	**Identifiers**	**Additional information**
antibody	anti-LRRK2 (mouse monoclonal)	Neuromab RRID:AB_2877351	N241A/34	(1:1000)
antibody	anti-LRRK2 phospho S935 (rabbit monoclonal)	Abcam RRID:AB_2904231	UDD2	(1:1000)
antibody	anti-Rab10 (mouse monoclonal)	Nanotools RRID:AB_2921226	0680–100/Rab10-605B11	(1:1000)
antibody	anti-Rab10 (phospho T73) (rabbit monoclonal)	Abcam RRID:AB_2811274	ab230261	(1:1000)
antibody	anti-FLAG M2 (mouse monoclonal)	Millipore Sigma RRID:AB_262044	F-1804	(1:2000)
strain, strain background (*Escherichia coli*)	E. coli DH5α	Thermo Fisher	18258012	
strain, strain background (*Escherichia coli*)	E. coli STBL3	Thermo Fisher	C737303	
strain, strain background (*Escherichia coli*)	E. coli Rosetta DE3 pLys	Millipore	70956	
cell line (*Homo-sapiens*)	HeLa	ATCC	CCL-2	
cell line (*Homo-sapiens*)	HEK293T	ATCC	CRL-3216	
Chemical compound, drug	MLi-2	MRC PPU		
Chemical compound, drug	Creatine Phosphate	Fluka Analytical	#27920	20mM
Commercial assay, kit	RED-NHS 2nd Generation (Amine Reactive) Protein Labeling Kit	Nanotemper Technologies	MO-L011	
Commercial assay, kit	CF® 633 Succinimidyl Ester Protein Labeling Kit	Biotium	#92217	
Other	Creatine Phosphokinase	Sigma	C3755	30U

Chemical compound, drug	18:1 (Δ9-Cis) PC (DOPC)	Avanti Polar Lipids	#850375	11 µmol
Chemical compound, drug	18:1 PS (DOPS)	Avanti Polar Lipids	#840035	5 µmol
Chemical compound, drug	18:1 DGS-NTA(Ni)	Avanti Polar Lipids	#790404	0.85 µmol
Chemical compound, drug	18:1 PI(4)P	Avanti Polar Lipids	#850151	0.15 µmol
Chemical compound, drug	DiD	Thermo Fisher	D7757	0.01 µmol
recombinant DNA reagent	pNIC Bsa-4 His-Sumo Rab10 Q68L 1-181	gift of Amir Khan		human
recombinant DNA reagent	pET15b His-Mst3	gift of Amir Khan		human
recombinant DNA reagent	pET21b GFP-Rab10 Q68L-His	Addgene RRID:Addgene_186015	186015	human
recombinant DNA reagent	pET21b His Rab8A Q67L	Addgene RRID:Addgene_186014	186014	human
recombinant DNA reagent	pQE-80L 2xHis-Rab29	Addgene RRID:Addgene_186021	186021	human
recombinant DNA reagent	pGEB GST-Rab8A-Q67L	Addgene RRID:Addgene_86079	86079	human
recombinant DNA reagent	His-Rab11	gift of Marino Zerial		canine
recombinant DNA reagent	pQE-80L 2xHis-LRRK2 Armadillo 1-552	Addgene RRID:Addgene_186017	186017	human
recombinant DNA reagent	pQE-80L 2xHis-LRRK2-Armadillo 1-159	Addgene RRID:Addgene_186016	186016	human
recombinant DNA reagent	pQE-80L 2xHis-LRRK2-Armadillo 350-550	Addgene RRID:Addgene_186018	186018	human
recombinant DNA reagent	pQE-80L 2xHis-LRRK2-Armadillo K17A	Addgene RRID:Addgene_186019	186019	human
recombinant DNA reagent	pQE-80L 2xHis-LRRK2-Armadillo K18A	Addgene RRID:Addgene_186020	186020	human
recombinant DNA reagent	pCMV5 FLAG-LRRK2 K17A/K18A/R1441G	Addgene RRID:Addgene_186012	186012	human
recombinant DNA reagent	pCMV5 FLAG-LRRK2	MRC PPU Reagents and Services, University of Dundee ("MRC PPU")	DU6841	human
recombinant DNA reagent	pCMV5 FLAG-LRRK2 R1441G	MRC PPU	DU13077	human
recombinant DNA reagent	pCMV5 FLAG-LRRK2 D2017A	MRC PPU	DU52725	human

recombinant DNA reagent	pcDNA5D FRT TO GFP LRRK2 WT	MRC PPU	DU13363	Human
recombinant DNA reagent	pcDNA5D FRT TO GFP LRRK2 R361E	MRC PPU	DU62605	Human
recombinant DNA reagent	pcDNA5D FRT TO GFP LRRK2 D392K	MRC PPU	DU72261	Human
recombinant DNA reagent	pcDNA5D FRT TO GFP LRRK2 R399E	MRC PPU	DU72262	Human
recombinant DNA reagent	pcDNA5D FRT TO GFP LRRK2 L403A	MRC PPU	DU72263	Human
recombinant DNA reagent	pcDNA5D FRT TO GFP LRRK2 L406A	MRC PPU	DU72266	Human
recombinant DNA reagent	pcDNA5D FRT TO GFP LRRK2 M407A	MRC PPU	DU72267	Human
recombinant DNA reagent	pcDNA5D FRT TO GFP LRRK2 K439E	MRC PPU	DU72268	Human
recombinant DNA reagent	pcDNA5D FRT TO GFP LRRK2 L443A	MRC PPU	DU72270	Human
recombinant DNA reagent	pcDNA5D FRT TO GFP LRRK2 K451E	MRC PPU	DU72271	Human
recombinant DNA reagent	pcDNA5D FRT TO GFP LRRK2 D478Y	MRC PPU	DU68605	Human
recombinant DNA reagent	pcDNA5D FRT TO GFP LRRK2 D2017A	MRC PPU	DU13364	Human
recombinant DNA reagent	pcDNA5D FRT TO GFP LRRK2 R1441C	MRC PPU	DU13387	Human
recombinant DNA reagent	pcDNA5D FRT TO GFP LRRK2 R1441C R361E	MRC PPU	DU72304	Human
recombinant DNA reagent	pcDNA5D FRT TO GFP LRRK2 R1441C D392K	MRC PPU	DU72305	Human
recombinant DNA reagent	pcDNA5D FRT TO GFP LRRK2 R1441C R399E	MRC PPU	DU72306	Human
recombinant DNA reagent	pcDNA5D FRT TO GFP LRRK2 R1441C L403A	MRC PPU	DU72307	Human
recombinant DNA reagent	pcDNA5D FRT TO GFP LRRK2 R1441C L406A	MRC PPU	DU72308	Human
recombinant DNA reagent	pcDNA5D FRT TO GFP LRRK2 R1441C M407A	MRC PPU	DU72309	Human
recombinant DNA reagent	pcDNA5D FRT TO GFP LRRK2 R1441C K439E	MRC PPU	DU72310	Human
recombinant DNA reagent	pcDNA5D FRT TO GFP LRRK2 R1441C L443A	MRC PPU	DU72311	Human
recombinant DNA reagent	pcDNA5D FRT TO GFP LRRK2 R1441C K451E	MRC PPU	DU72312	Human
recombinant DNA reagent	pCMV5D HA RAB29	MRC PPU	DU50222	Human

recombinant DNA reagent	pcDNA5D FRT TO GFP LRRK2 1-950	MRC PPU	DU62702	Human
recombinant DNA reagent	pcDNA5D FRT TO GFP LRRK2 1-900	MRC PPU	DU62701	Human
recombinant DNA reagent	pcDNA5D FRT TO GFP LRRK2 1-850	MRC PPU	DU62700	Human
recombinant DNA reagent	pcDNA5D FRT TO GFP LRRK2 1-800	MRC PPU	DU62693	Human
recombinant DNA reagent	pcDNA5D FRT TO GFP LRRK2 1-750	MRC PPU	DU62726	Human
recombinant DNA reagent	pcDNA5D FRT TO GFP LRRK2 1-700	MRC PPU	DU62689	Human
recombinant DNA reagent	pcDNA5D FRT TO GFP LRRK2 1-650	MRC PPU	DU62678	Human
recombinant DNA reagent	pcDNA5D FRT TO GFP LRRK2 1-600	MRC PPU	DU62677	Human
recombinant DNA reagent	pcDNA5D FRT TO GFP LRRK2 1-550	MRC PPU	DU62676	Human
recombinant DNA reagent	pcDNA5D FRT TO GFP LRRK2 1-500	MRC PPU	DU62675	Human
recombinant DNA reagent	pcDNA5D FRT TO GFP LRRK2 50-1000	MRC PPU	DU62725	Human
recombinant DNA reagent	pcDNA5D FRT TO GFP LRRK2 100-1000	MRC PPU	DU62742	Human
recombinant DNA reagent	pcDNA5D FRT TO GFP LRRK2 150-1000	MRC PPU	DU62674	Human
recombinant DNA reagent	pcDNA5D FRT TO GFP LRRK2 200-1000	MRC PPU	DU62679	Human
recombinant DNA reagent	pcDNA5D FRT TO GFP LRRK2 250-1000	MRC PPU	DU62680	Human
recombinant DNA reagent	pcDNA5D FRT TO GFP LRRK2 300-1000	MRC PPU	DU62681	Human
recombinant DNA reagent	pcDNA5D FRT TO GFP LRRK2 350-1000	MRC PPU	DU62682	Human
recombinant DNA reagent	pcDNA5D FRT TO GFP LRRK2 400-1000	MRC PPU	DU62683	Human
recombinant DNA reagent	pcDNA5D FRT TO GFP LRRK2 450-1000	MRC PPU	DU62684	Human
recombinant DNA reagent	pcDNA5D FRT TO GFP LRRK2 500-1000	MRC PPU	DU62685	Human
recombinant DNA reagent	pcDNA5D FRT TO GFP LRRK2 550-1000	MRC PPU	DU62686	Human
recombinant DNA reagent	pcDNA5D FRT TO GFP LRRK2 600-1000	MRC PPU	DU62687	Human
recombinant DNA reagent	pcDNA5D FRT TO GFP LRRK2 350-550	MRC PPU	DU68397	Human

recombinant DNA reagent	pcDNA5D FRT TO GFP LRRK2 350-500	MRC PPU	DU68398	Human
recombinant DNA reagent	His-SUMO Rab10	MRC PPU	DU51062	Human
recombinant DNA reagent	His Rab7	Gift of Marino Zerial		
software, algorithm	FIJI	PMID: 29187165	RRID:SCR_002285	
software, algorithm	CellProfiler	PMID: 29969450	RRID:SCR_007358	
software, algorithm	TrackIt	PMID: 33947895		
software, algorithm	Chimera 2	PMID:15264254	RRID:SCR_004097	
software, algorithm	Chimera X	PMID: 32881101	RRID:SCR_015872	
software, algorithm	Nanotemper NTAAffinityAnalysis	MO.Affinity Analysis v2.2.5		
software, algorithm	Prism	Prism 9 version 9.3.1 (350)	RRID:SCR_002798	
software, algorithm	R CRAN R package Dplyr_1.0.9 ggridges_0.5.3 ggplot_3.3.6	version 4.2.0 (2022-04-22)	RRID:SCR_003005 version 4.2.0 (2022-04-22)	

415

416 **Methods**

417 **Cloning and plasmids**

418 DNA constructs were amplified in Escherichia coli DH5α or STBL3 and purified using mini prep
419 columns (Econospin). DNA sequence verification was performed by Sequetech
420 (http://www.sequetech.com). pNIC Bsa-4 His-Sumo Rab10 Q68L 1-181 and pET15b His-
421 Mst3 were kind gifts of Amir Khan (Harvard University). pET21b GFP-Rab10 Q68L-His was
422 subcloned from GFP-Rab10 (Gomez et al. 2019) into pET21b. The C-terminal His tagged
423 version was generated by Gibson assembly. His Rab8A Q67L was subcloned from HA-Rab8A
424 (DU35414, Medical Research Council at Dundee) into pET14b. Point mutations were generated
425 using site directed mutagenesis. His-Rab29 wild type was subcloned from HA-Rab29 (DU5022,
426 Medical Research Council at Dundee) into the pQE-80L backbone. pCMV5 FLAG-LRRK2
427 (DU6841), Flag-LRRK2 R1441G (DU13077), His-SUMO Rab10 (DU51062) and FLAG-LRRK2
428 D2017A (DU52725) were obtained from the Medical Research Council at Dundee. His-
429 Armadillo 1-552, 1-159, and 350-550 were all cloned from pCMV5 FLAG-LRRK2 into pQE-80L.
430 K17A, K18A, and K17A/K18A LRRK2 and LRRK2 Armadillo were generated using site directed
431 mutagenesis. All cloning and subcloning was done by Gibson assembly.

432 **Rab GTPase, LRRK2 Armadillo domain, and LRRK2 purification**

433 His Rab29, His Rab10-Q68L (1–181), His-Mst3, His-Rab8A Q67L, His-LRRK2 Armadillo (1-
434 552), His-LRRK2 Armadillo (1-159), His-LRRK2 Armadillo (350-550), His-LRRK2 Armadillo
435 K17A, His-LRRK2 Armadillo K18A, and GST-Rab8A Q67L were purified in E.coli BL21 (DE3
436 pLys). Detailed protocols can be found in Gomez et al., 2020
437 https://dx.doi.org/10.17504/protocols.io.bffrjjm6 and Vides et al., 2021
438 https://dx.doi.org/10.17504/protocols.io.bvvmn646. Bacterial cells were grown at 37°C in Luria
439 Broth and induced at A600 nm = 0.6–0.7 by the addition of 0.3 mM isopropyl-1-thio-β-D-
440 galactopyranoside (Gold Biotechnology) and harvested after 18 h at 18°C. The cell pellets were
441 resuspended in ice cold lysis buffer (50 mM HEPES, pH 8.0, 10% [vol/vol] glycerol, 500 mM
442 NaCl,10 mM imidazole (for His-tagged purification only), 5 mM $MgCl_2$, 0.2mM tris(2-
443 carboxyethyl) phosphine (TCEP), 20 µM GTP, and EDTA-free protease inhibitor cocktail
444 (Roche). The resuspended bacteria were lysed by one passage through an Emulsiflex-C5
445 apparatus (Avestin) at 10,000 lbs/in^2 and centrifuged at 40,000 rpm for 45 min at 4°C in a
446 Beckman Ti45 rotor. Cleared lysate was filtered through a 0.2µm filter (Nalgene) and passed
447 over a HiTrap TALON crude 1mL column (Cytiva) for His-tagged proteins or a GSTrap High
448 Performance 1 mL column (Cytiva) for GST-tagged proteins. The column was washed with lysis
449 buffer until absorbance values reached pre-lysate values. Protein was eluted with a gradient
450 from 20-500 mM imidazole containing lysis buffer for His-tagged proteins or 0-50 mM reduced
451 glutathione containing lysis buffer for GST-tagged proteins. Peak fractions analyzed by 10%
452 SDS-PAGE to locate protein. The eluate was buffer exchanged and further purified by gel
453 filtration on Superdex-75 (GE Healthcare) with 50 mM HEPES, pH 8, 5% (vol/vol) glycerol, 150
454 mM NaCl, 5 mM $MgCl_2$, 0.1 mM tris(2-carboxyethyl) phosphine (TCEP), and 20 µM GTP.

455 LRRK2 R1441G was transfected into HEK293T cells with Polyethylenimine HCl MAX 4000
456 (PEI) (Polysciences, Inc.) and purified 48hrs post transfection. Cells were lysed in 50mM Hepes
457 pH 8, 150mM NaCl, 1mM EDTA, 0.5% Triton-X 100, 10% (vol/vol) glycerol and protease
458 inhibitor cocktail (Roche). Lysate was centrifuged at 15,000g for 20min in Fiberlite F15 rotor
459 (ThermoFischer). Clarified lysate was filtered through 0.2µm syringe filters and circulated over
460 anti-FLAG M2 affinity gel (Sigma) at 4°C for 4hrs using a peristaltic pump. The affinity gel was
461 washed with 6 column volumes of lysis buffer followed by 6 column volumes of elution buffer
462 (50mM Hepes pH 8, 150mM NaCl, and 10% [vol/vol] glycerol). Protein was eluted from resin

463 with 5 column volumes of FLAG peptide (0.25mg/mL) containing elution buffer. Eluate was
464 supplemented to 20μM GTP, 1mM ATP, and 2mM $MgCl_2$.

465 **In vitro Rab phosphorylation and microscale thermophoresis**

466 A detailed method can be found at https://dx.doi.org/10.17504/protocols.io.bvvmn646). His-
467 Rab10 Q68L 1–181 or His-Rab8A Q67L was incubated with His-Mst3 kinase at a molar ratio of
468 3:1 (substrate:kinase). The reaction buffer was 50 mM Hepes, pH 8, 5% (vol/vol) glycerol, 100
469 mM NaCl, 5 mM $MgCl_2$, 0.2 mM TCEP, 20 μM GTP, 5 μM BSA, 0.01% Tween-20, and 2 mM
470 ATP (no ATP for negative control). The reaction mixture was incubated at 27°C for 30 min in a
471 water bath. Phosphorylation completion was assessed by Western blot. Immediately after
472 phosphorylation, the samples were transferred to ice before binding determination. See also
473 https://dx.doi.org/10.17504/protocols.io.bvjxn4pn.

474 Protein–protein interactions were monitored by microscale thermophoresis using a Monolith
475 NT.115 instrument (Nanotemper Technologies). His LRRK2 Armadillo (1-552), (1-159), (350-
476 550), K17A and K18A were labeled using RED-NHS 2nd Generation (Amine Reactive) Protein
477 Labeling Kit (Nanotemper Technologies). For all experiments, the unlabeled protein partner was
478 titrated against a fixed concentration of the fluorescently labeled LRRK2 Armadillo (100 nM); 16
479 serially diluted titrations of the unlabeled protein partner were prepared to generate one
480 complete binding isotherm. Binding was carried out in a reaction buffer in 0.5-ml Protein LoBind
481 tubes (Eppendorf) and allowed to incubate in the dark for 30 min before loading into NT.115
482 premium treated capillaries (Nanotemper Technologies). A red LED at 30% excitation power
483 (red filter, excitation 605–645 nm, emission 680–685 nm) and IR-laser power at 60% was used
484 for 30 s followed by 1 s of cooling. Data analysis was performed with NTAffinityAnalysis
485 software (NanoTemper Technologies) in which the binding isotherms were derived from the raw
486 fluorescence data and then fitted with both NanoTemper software and GraphPad Prism to
487 determine the K_D using a non-linear regression method. The binding affinities determined by the
488 two methods were similar. Shown are averaged curves of Rab GTPase binding partners from
489 single readings from two different protein preparations. Note that the affinities reported here are
490 underestimates as preps of His Rab10-Q68L (1–181) and His-Rab8A Q67L routinely contained
491 a 50:50 ratio of bound GTP:GDP as determined by mass spectroscopy; data were not corrected
492 for this.

493 **Cell culture and Immunoblotting**

494 HEK293T and HeLa cells were obtained from American Type Culture Collection were cultured
495 at 37°C and under 5% CO2 in Dulbecco's modified Eagle 's medium containing 10% fetal
496 bovine serum, 2 mM Glutamine, and penicillin (100 U/ml)/streptomycin (100 μg/ml). HEK293T
497 and HeLa cells were transfected with polyethylenimine HCl MAX 4000 (Polysciences). Cells
498 were routinely checked for Mycoplasma by PCR analysis.

499 HeLa cells for pRab10 recovery kinetics were lysed 48 hr post transfection and MLi-2 treatment
500 in ice cold lysis buffer (50mM Tris pH 7.4, 150mM NaCl, 0.5% Triton X-100, 5mM $MgCl_2$, 1 mM
501 sodium orthovanadate, 50 mM NaF, 10 mM 2-glycerophosphate, 5 mM sodium pyrophosphate,
502 0.1 μg/ml mycrocystin-LR (Enzo Life Sciences), and EDTA-free protease inhibitor cocktail
503 (Sigma-Aldrich). Lysates were centrifuged at 14,000g for 15 min at 4°C and supernatant protein
504 concentrations were determined by Bradford assay (Bio-Rad).

505 A detailed protocol for blotting is available on protocols.io (Tonelli and Alessi,
506 https://dx.doi.org/10.17504/protocols.io.bsqrnbv6). 20μg of protein were run on SDS PAGE gels
507 and transferred onto nitrocellulose membranes using a Bio-Rad Trans-turbo blot system.
508 Membranes were blocked with 2% BSA in Tris-buffered saline with Tween-20 for 30 at RT.

509 Primary antibodies used were diluted in blocking buffer as follows: mouse anti-LRRK2
510 N241A/34 (1:1000, Neuromab); rabbit anti-LRRK2 phospho S935 (1:1000, Abcam); mouse anti-
511 Rab10 (1:1000, Nanotools); and rabbit anti-phospho Rab10 (1:1000, Abcam). Primary antibody
512 incubations were done overnight at 4°C. LI-COR secondary antibodies diluted in blocking buffer
513 were 680 nm donkey anti-rabbit (1:5,000) and 800 nm donkey anti-mouse (1:5,000). Secondary
514 antibody incubations were for 1 h at RT. Blots were imaged using an Odyssey Infrared scanner
515 (LI-COR) and quantified using ImageJ software.

516 **MLi-2 washout/ pRab10 recovery kinetics**

517 As described by Ito et al. (2016), HeLa cell seeded in 6x 60mm dishes expressing FLAG-
518 LRRK2, LRRK2 K17A/K18A, LRRK2 R1441G, or LRRK2 R1441G/K17A/K18A for 48 hours
519 were incubated with 200nm MLi-2 or DMSO for 1 hour under normal growth conditions at 37°C.
520 To remove the MLi-2 inhibitor, cells were washed 4 times with complete media. Washouts were
521 done to allow for 120-15 min of enzyme activity recovery; after which, cells were harvested.

522 **Confocal light microscopy**

523 The standard method to obtain images in Figure 3 and Figure 3 supplements can be found on
524 protocols.io (Purlyte et al., 2022 https://dx.doi.org/10.17504/protocols.io.b5jhq4j6). For Figure 8,
525 cells were plated onto collagen coated coverslips with indicated plasmids. Cells were washed
526 with ice cold phosphate buffered saline (PBS) 3x. After, they were incubated in glutamate buffer
527 (25mM KCl, 25mM Hepes pH7.4, 2.5mM magnesium acetate, 5mM EGTA, and 150mM K
528 glutamate) for 5 min on ice. Coverslips were dipped into liquid nitrogen and held for 5 sec before
529 removal. They were thawed at RT, incubated in glutamate buffer for 2 min and then in PBS for 5
530 min. Cells were fixed with 3.5% paraformaldehyde in PBS for 15 min, permeabilized for 3 min in
531 0.1% Triton X-100, and blocked with 1% BSA in PBS. Antibodies were diluted as follows: mouse
532 anti-FLAG (1:2000, Sigma-Aldrich) and rabbit anti pRab10 (1:2000; Abcam). Highly cross-
533 absorbed H+L secondary anti-bodies (Life Technologies) conjugated to Alexa Fluor 568 or 647
534 were used at 1:2,000. Images were obtained using a spinning disk confocal microscope
535 (Yokogawa) with an electron multiplying charge coupled device camera (Andor) and a 100× 1.4
536 NA oil immersion objective. Mander's correlation coefficients were calculated by analyzing
537 maximum intensity projection images with CellProfiler software (Carpenter et al., 2006; Stirling
538 et al., 2021).

539 Co-localization of Rab29 with full length LRRK2 and its mutants was quantified using an
540 unbiased Cellprofiler pipeline as follows: Step 1. Imported raw .lsm files; 2. metadata extracted
541 from the file headers; 3. images grouped by mutations and split into 3 channels; 4. nuclei
542 identified as primary objects after rescaling intensities; 5. Nucleus is defined as the primary
543 object and cells are identified by 'propagation' as secondary objects; cells are identified as the
544 using the rescaled and smoothened LRRK2 channel. 6. Co-localization within whole cells is
545 measured by thresholded (10) Mander's coefficient on the entire batch of images. Data plotted
546 from Cellprofiler are relative values.

547 **Substrate supported lipid bilayer preparation**

548 A detailed method can be found at dx.doi.org/10.17504/protocols.io.x54v9y7qzg3e/v1. Briefly,
549 we used Lab-TeKII 8 chambered No. 1.5 borosilicate cover glasses (Fischer) for LRRK2
550 recruitment assays. Reactions chambers were cleaned by 30 min incubation in Piranha solution
551 (1:3 [vol/vol] ratio of 30% H_2O_2 and 98% H_2SO_4) and extensive washing in Milli-Q water. The
552 reaction chambers were stored in Milli-Q water for up to 2 weeks. Before use, reaction
553 chambers were dried and further cleaned in a Harrick Plasma PDC-32C plasma cleaner for 10
554 min at 18W under ambient air.

555 We prepared substrate supported lipid bilayers on glass coverslips with 65% DOPC, 29%
556 DOPS, 5% DOGS-NTA[Ni^2], 1% PI(4)P, 0.01% DIL (Avanti Polar Lipids;Thermo). The lipid
557 mixture was suspended in 1ml chloroform and then dried under nitrogen flow in a glass vial and
558 kept under vacuum for at least 1 h. The dried lipids were hydrated in SLB buffer (20 mM Hepes
559 pH 8, 150 mM potassium acetate, 1 mM $MgCl_2$) by vortexing to produce multilamellar vesicles
560 (MLVs). SUVs were prepared by bath sonication followed by extrusion through 100 nm
561 polycarbonate membrane 21 times (Avestin). The produced SUVs were stored at -20°C. The
562 supported lipid bilayer was formed in cleaned reaction chambers on glass surfaces by addition
563 of liposomes to a final concentration of 5mM liposomes in SLB buffer. SUV fusion was induced
564 by addition of 1mM $CaCl_2$ and incubated for 45 min at 37°C. Next, the unfused vesicles were
565 washed with Milli-Q water and STD buffer (20mM Hepes pH 8, 150mM NaCl, 5mM $MgCl_2$).

566 Lab-TeKII 8 chambered No. 1.5 borosilicate coverglass (Fisher) were coated with Poly-D-lysine
567 as follows (Adhikari et al., 2022). 10 mg Poly-D-lysine (MPBio # SKU:02150175-CF) was
568 dissolved in 1ml of sterile Milli-Q water as a 1% stock solution. The stock solution was then
569 diluted two fold in PBS as 1X coating solution. Coating solution (200µl) was added to the
570 reaction chamber and incubated for 5 min at 37°C. The coating solution was then removed by
571 rinsing the chamber thoroughly with sterile Milli-Q water and equilibrated with reaction buffer
572 (20mM Hepes pH8; 150mM NaCl, 5mM MgCl2, 4mM ATP, 20µM GTP, 20 mM creatine
573 phosphate, 30U creatine phosphokinase)
574 (dx.doi.org/10.17504/protocols.io.x54v9y7qzg3e/v1).
575
576 **TIRF microscopy**

577 A detailed method can be found on protocols.io (Adhikari et al., 2022
578 dx.doi.org/10.17504/protocols.io.x54v9y7qzg3e/v1). All LRRK2 recruitment movies were
579 obtained at 25°C, at a frame rate capture interval of 1 sec using a Nikon Ti-E inverted
580 microscope with the Andor iXon+EMCCD camera model DU885 with PerfectFocus and a Nikon
581 TIRF Apo 100x 1.46 NA oil immersion objective. The imaging was done with 300 EM camera
582 gain and 50 ms exposure time with 200µW laser intensity. We analyzed the microscopy data
583 with TrackIt (Kuhn T., et al., 2021) to obtain spot density of bound LRRK2.
584

585 **Rab10-dependent LRRK2 recruitment**

586 A detailed method can be found on protocols.io (Adhikari et al., 2022
587 dx.doi.org/10.17504/protocols.io.x54v9y7qzg3e/v1). Purified FLAG LRRK2 is labeled with
588 CF633 succinimidyl ester (Biotium 92217) by incubation with dye for 1 hr at RT in the dark.
589 After dye removal using Pierce Dye Removal Columns (Thermo Scientific #22858),
590 protein was determined by Bradford Assay. Labeling efficiency was determined using
591 the dye extinction coefficient and preps were labeled with 2-3 moles of dye per mole
592 LRRK2 for all experiments.
593 GFP Rab10 Q68L C-terminal His was added to supported lipid bilayers at a final concentration
594 of 2.5µM in STD buffer and incubated for 20 min at 37°C. After incubation, Rab coated
595 supported lipid bilayers were washed with STD buffer and then equilibrated with reaction buffer
596 (20mM Hepes pH 8, 150mM NaCl, 5mM $MgCl_2$, 4mM ATP, 20µM GTP, 20mM creatine
597 phosphate, 30U creatine phosphokinase). 14nM CF633-FLAG LRRK2 was prepared in reaction
598 buffer and allowed to equilibrate to RT for 5 min. 40 sec into imaging, 100µL from the 200uL in
599 the reaction chamber was removed. At 60 sec, 100µL of 14nM CF FLAG LRRK2 was added
600 and imaged for 600 sec and for 300 sec for no Rab10 control.

601 **LRRK2 Kinase Activation Assay**
602 Method #1. Purified His-Rab8A Q67L (0.5 mg) was phosphorylated using His-MST3 kinase
603 (0.1-0.3 mg) as described above at 30°C overnight in MST3 reaction buffer (50 mM HEPES, pH
604 8, 5% (v/v) glycerol, 150 mM NaCl, 5 mM $MgCl_2$, 0.2 mM TCEP, 20 μM GTP, 5 μM BSA, 0.01%
605 Tween-20, and 2 mM ATP). Phosphorylated Rab8A (25 kDa) was then resolved from MST3 (55
606 kDa) by gel filtration on a 24 mL Superdex 75 10/300 column (Cytiva Life Sciences, #17517401.
607 An additional Method #2 was attempted to try to further remove trace MST3 from phosphoRab8.
608 GST-PreScission protease was bound to glutathione agarose. His-MST3 was added to the
609 beads and incubated overnight at 4°C. The supernatant containing free MST3 was then
610 passed through a Nickel-NTA column to remove any uncleaved His-MST3. The pooled,
611 untagged, MST3 supernatants were then used to phosphorylate His-Rab8A. The products of
612 this reaction were gel filtered on Superdex 75 column as before, and phosphorylated His-Rab8A
613 was then further purified by immobilization on nickel-NTA agarose, eluted with 500 mM
614 imidazole after washing, and desalted as described above.
615
616 LRRK2 G2019S (88 nM; Thermo Fisher Scientific #A15200) or purified FLAG-LRRK2 R1441G
617 K18A (Adhikari et al., 2022) was incubated with 3 μM His-GFP-Rab10 Q68L (1-181) or His-
618 SUMO-Rab10 wild type full length substrate ± 6 μM phosphorylated Rab8A Q67L in 50 mM
619 HEPES pH 8, 5% (v/v) glycerol, 150 mM NaCl, 10 mM $MgCl_2$, 250 μM GTP, 5 μM BSA, and 2
620 mM ATP. No difference was detected between the two Rab10 substrates. The reaction was
621 incubated at 30°C in a water bath. Reactions were stopped by the addition of SDS-PAGE
622 sample buffer; MLi-2 (200nM) was added to control reactions. Samples were analyzed by SDS-
623 PAGE and immunoblotted for phosphoRab10. Blots were imaged using Li-COR and bands
624 quantified using ImageJ. The values obtained with MLi-2 were subtracted from their respective
625 timepoints to monitor LRRK2-dependent phosphorylation; background was due to trace residual
626 MST kinase. Values from four independent, replicate experiments were normalized to the 20
627 min time point and plotted together using GraphPad Prism.
628
629 **Dual Rab GTPase Binding to the LRRK2 Armadillo Domain**
630 The strategy was to immobilize Rab8A, bind Armadillo domain, and then test if Rab8A-tethered
631 Armadillo domain could simultaneously bind phosphoRab10. His-Rab10 Q68L 1-181 was pre-
632 phosphorylated with His-MST3 kinase at a molar ratio of 3:1 (substrate:kinase) at 30°C for 2
633 hours in MST3 reaction buffer. 50 μL glutathione agarose slurry was pelleted and resuspended
634 in 50 mM HEPES, pH 8, 5% (v/v) glycerol, 150 mM NaCl, 5 mM $MgCl_2$, 0.2 mM TCEP, 100 μM
635 GTP, 5 μM BSA, 0.01% Tween-20 to achieve a total volume of 50 μL. GST-Rab8A Q67L (6μM
636 in 50μl) was incubated with glutathione beads in reaction buffer for 30 min at room temperature
637 (RT) on a rotator. The reaction was spun down at 3200 x g for 30 sec and the supernatant
638 discarded. His-LRRK2 Armadillo domain 1-552 in reaction buffer (or buffer alone) was added to
639 beads to achieve a final concentration of 10 μM in 50 μL and incubated for 30 min at RT on a
640 rotator. The reaction was spun down as before and the supernatant discarded. Phosphorylated
641 His-Rab10 Q68L 1-181 (4μM final) were added to beads in a final volume of 50 μl. Reactions
642 were incubated for 30 min at RT on a rotator. The reaction was spun down at 3200 xg for 30
643 seconds and the supernatant discarded; reaction buffer (500 μl) was used to wash the beads
644 twice. Proteins were eluted from the beads using 50 μl elution buffer (50 mM HEPES, pH 8, 5%
645 (v/v) glycerol, 150 mM NaCl, 5 mM $MgCl_2$, 0.2 mM TCEP, 20 μM GTP, 50 mM reduced
646 glutathione). The reaction was spun down at 3200 xg for 30 sec and the supernatant was
647 collected. Samples were then analyzed by SDS-PAGE and immunoblotted for phosphoRab10.
648 Blots were imaged using Li-COR, and bands were quantified using ImageJ.

649 **Intensity analysis of TIRF videos.** Tracks of individual molecules were extracted from TIRF
650 microscopy images using the TrackIT FiJi plugin and converted to .csv files using the custom

"getTracks.m" Matlab script (https://github.com/PfefferLab/Vides_et_al_2022). These files were loaded as data frames in R and processed with dplyr for the binning and normalization steps. Pre-normalized intensities I_t were obtained from the amplitude value fitted by TrackIT (backround corrected amplitude of the Gaussian fit of each particle). Ridge plots were produced using the ggridges package with a Gaussian Kernel density and a bandwidth of 0.2. Code used to generate each figure is available on GitHub (https://github.com/PfefferLab/Vides_et_al_2022).

Acknowledgements

This study was funded by the joint efforts of The Michael J. Fox Foundation for Parkinson's Research (MJFF) [17298 & 6986 (S.R.P. & D.R.A.)] and Aligning Science Across Parkinson's (ASAP) initiative. MJFF administers the grant (ASAP-000463, S.R.P. & D.R.A.) on behalf of ASAP and itself. Funds were also provided by the Medical Research Council [grant no. MC_UU_00018/1 (D.R.A.), the pharmaceutical companies supporting the Division of Signal Transduction Therapy Unit (Boehringer-Ingelheim, GlaxoSmithKline, Merck KGaA (D.R.A.), and a Ph.D. fellowship from Consejería de Economía, Conocimiento y Empleo del Gobierno de Canarias in partnership with Fondo Social Europeo (E.S-L.).

For the purpose of open access, the authors have applied a CC-BY public copyright license to the Author Accepted Manuscript version arising from this submission. All primary data associated with each figure has been deposited in a repository and can be found at https://doi.org/10.5061/dryad.3tx95x6j7; quantitation data of the blots in Figure 3--Fig. Supp. 4 (for the bar graphs in Figures 3C and 3D) can be found at doi (10.5281/zenodo.7057419).

We are especially grateful to Dr. Gheorghe Chistol for helpful discussion and Chloe Rollock for help with protein purification. We also thank the excellent technical support of the MRC protein phosphorylation and ubiquitylation unit (PPU) DNA sequencing service (coordinated by Gary Hunter), the MRC-PPU tissue culture team (coordinated by Edwin Allen), MRC-PPU Reagents and Services antibody and protein purification teams (coordinated by Dr James Hastie).

682 **References**

683 Adhikari, A, Vides, E. and Pfeffer, S.R. 2022. Reconstitution of LRRK2 membrane
684 recruitment onto planar lipid bilayers. dx.doi.org/10.17504/protocols.io.x54v9y7qzg3e/v1

685 Alessi DR, Sammler E. LRRK2 kinase in Parkinson's disease. Science. 2018 Apr
686 6;360(6384):36-37. doi: 10.1126/science.aar5683.

687 Ashkenazy H, Abadi S, Martz E, Chay O, Mayrose I, Pupko T, Ben-Tal N. ConSurf 2016: an
688 improved methodology to estimate and visualize evolutionary conservation in macromolecules.
689 Nucleic Acids Res. 2016 Jul 8;44(W1):W344-50.

690 Barbero P, Bittova L, Pfeffer SR. Visualization of Rab9-mediated vesicle transport from
691 endosomes to the trans-Golgi in living cells. J Cell Biol. 2002 Feb 4;156(3):511-8

692 Berger Z, Smith KA, Lavoie MJ. Membrane localization of LRRK2 is associated with increased
693 formation of the highly active LRRK2 dimer and changes in its phosphorylation. Biochemistry.
694 2010 Jul 6;49(26):5511-23.

695 Berndsen K, Lis P, Yeshaw WM, Wawro PS, Nirujogi RS, Wightman M, Macartney T, Dorward
696 M, Knebel A, Tonelli F, Pfeffer SR, Alessi DR. PPM1H phosphatase counteracts LRRK2
697 signaling by selectively dephosphorylating Rab proteins. Elife. 2019 Oct 30;8:e50416. doi:
698 10.7554/eLife.50416.

699 Biskup S, Moore DJ, Celsi F, Higashi S, West AB, Andrabi SA, Kurkinen K, Yu SW, Savitt JM,
700 Waldvogel HJ, Faull RL, Emson PC, Torp R, Ottersen OP, Dawson TM, Dawson VL.
701 Localization of LRRK2 to membranous and vesicular structures in mammalian brain. Ann
702 Neurol. 2006 Nov;60(5):557-69.

703 Boecker CA, Goldsmith J, Dou D, Cajka GG, Holzbaur ELF. Increased LRRK2 kinase activity
704 alters neuronal autophagy by disrupting the axonal transport of autophagosomes. Curr Biol.
705 2021 May 24;31(10):2140-2154.e6.

706 Civiero L, et al. (2012) Biochemical characterization of highly purified leucine-rich repeat
707 kinases 1 and 2 demonstrates formation of homodimers. PLoS One 7(8):e43472.

708 de Renzis S, Sönnichsen B, Zerial M. Divalent Rab effectors regulate the sub-compartmental
709 organization and sorting of early endosomes. Nat Cell Biol. 2002 Feb;4(2):124-33.

710 Deniston CK, Salogiannis J, Mathea S, et al. Structure of LRRK2 in Parkinson's disease and
711 model for microtubule interaction. *Nature*. 2020;588(7837):344-349. doi:10.1038/s41586-020-
712 2673-2

713 Dhekne HS, Yanatori I, Gomez RC, et al. A pathway for Parkinson's Disease LRRK2 kinase to
714 block primary cilia and Sonic hedgehog signaling in the brain. *Elife*. 2018;7:e40202. Published
715 2018 Nov 6. doi:10.7554/eLife.40202

716 Dhekne HS, Yanatori I, Vides EG, Sobu Y, Diez F, Tonelli F, Pfeffer SR. LRRK2-phosphorylated
717 Rab10 sequesters Myosin Va with RILPL2 during ciliogenesis blockade. Life Sci Alliance. 2021
718 Mar 16;4(5):e202101050. doi: 10.26508/lsa.202101050.

719 Gomez RC, Wawro P, Lis P, Alessi DR, Pfeffer SR. Membrane association but not identity is
720 required for LRRK2 activation and phosphorylation of Rab GTPases. J Cell Biol. 2019 Dec
721 2;218(12):4157-4170.

722 Gomez RC, Vides EG, Suzanne Pfeffer 2020. Rab29 fast exchange mutants: characterization of
723 a challenging Rab GTPase. **protocols.io** https://dx.doi.org/10.17504/protocols.io.bffrjjm6

724 Greggio E, Zambrano I, Kaganovich A, Beilina A, Taymans JM, Daniels V, Lewis P, Jain S, Ding
725 J, Syed A, Thomas KJ, Baekelandt V, Cookson MR. The Parkinson disease-associated leucine-
726 rich repeat kinase 2 (LRRK2) is a dimer that undergoes intramolecular autophosphorylation.
727 The Journal of biological chemistry. 2008;283:16906–16914.

728 Guaitoli G, Raimondi F, Gilsbach BK, Gómez-Llorente Y, Deyaert E, Renzi F, Li X, Schaffner A,
729 Jagtap PK, Boldt K, von Zweydorf F, Gotthardt K, Lorimer DD, Yue Z, Burgin A, Janjic N, Sattler
730 M, Versées W, Ueffing M, Ubarretxena-Belandia I, Kortholt A, Gloeckner CJ. Structural model of
731 the dimeric Parkinson's protein LRRK2 reveals a compact architecture involving distant
732 interdomain contacts. Proc Natl Acad Sci U S A. 2016 Jul 26;113(30):E4357-66.

733 Ito G, Katsemonova K, Tonelli F, Lis P, Baptista MA, Shpiro N, Duddy G, Wilson S, Ho PW, Ho
734 SL, Reith AD, Alessi DR. Phos-tag analysis of Rab10 phosphorylation by LRRK2: a powerful
735 assay for assessing kinase function and inhibitors. Biochem J. 2016 Sep 1;473(17):2671-85.

736 Itzhak DN, Tyanova S, Cox J, Borner GH. Global, quantitative and dynamic mapping of protein
737 subcellular localization. *Elife*. 2016;5:e16950. Published 2016 Jun 9. doi:10.7554/eLife.16950

738 Jumper J, Evans R, Pritzel A, Green T, Figurnov M, Ronneberger O, Tunyasuvunakool K, Bates
739 R, Žídek A, Potapenko A, Bridgland A, Meyer C, Kohl SAA, Ballard AJ, Cowie A, Romera-
740 Paredes B, Nikolov S, Jain R, Adler J, Back T, Petersen S, Reiman D, Clancy E, Zielinski M,
741 Steinegger M, Pacholska M, Berghammer T, Bodenstein S, Silver D, Vinyals O, Senior AW,
742 Kavukcuoglu K, Kohli P, Hassabis D. Highly accurate protein structure prediction with
743 AlphaFold. Nature. 2021 Aug;596(7873):583-589.

744 Jurrus E, Engel D, Star K, Monson K, Brandi J, Felberg LE, Brookes DH, Wilson L, Chen J,
745 Liles K, Chun M, Li P, Gohara DW, Dolinsky T, Konecny R, Koes DR, Nielsen JE, Head-Gordon
746 T, Geng W, Krasny R, Wei G-W, Holst MJ, McCammon JA, Baker NA. Improvements to the
747 APBS biomolecular solvation software suite. Protein Sci. 2018 Aug 24; 27 (1): 112-128.

748 Kalogeropulou AF, Freemantle JB, Lis P, Vides EG, Polinski NK, Alessi DR. Endogenous
749 Rab29 does not impact basal or stimulated LRRK2 pathway activity. Biochem J. 2020 Nov
750 27;477(22):4397-4423.

751 Klein CL, Rovelli G, Springer W, Schall C, Gasser T, Kahle PJ. Homo- and heterodimerization
752 of ROCO kinases: LRRK2 kinase inhibition by the LRRK2 ROCO fragment. J Neurochem 2009
753 Nov;111(3):703-15

754 Khan SS, Sobu Y, Dhekne HS, et al. Pathogenic LRRK2 control of primary cilia and Hedgehog
755 signaling in neurons and astrocytes of mouse brain. *Elife*. 2021;10:e67900. Published 2021 Oct
756 18. doi:10.7554/eLife.67900

Knebel A, Berndsen K, Lis P, Alessi DR. 2021. Expression and purification of Rab10 (1-181) stoichiometrically phosphorylated at Thr73 (the LRRK2 site). protocols.io https://dx.doi.org/10.17504/protocols.io.bvjxn4pn

Kuhn T, Hettich J, Davtyan R, Gebhardt JCM. (2021) Single molecule tracking and analysis framework including theory-predicted parameter settings. *Sci Rep.* 11(1):9465.

Kuwahara T, Inoue K, D'Agati VD, Fujimoto T, Eguchi T, Saha S, Wolozin B, Iwatsubo T, Abeliovich A. 2016. LRRK2 and RAB7L1 coordinately regulate axonal morphology and lysosome integrity in diverse cellular contexts. *SciRep* 6:29945

Liu Z, Bryant N, Kumaran R, et al. LRRK2 phosphorylates membrane-bound Rabs and is activated by GTP-bound Rab7L1 to promote recruitment to the trans-Golgi network. Hum Mol Genet. 2018;27:385–395.

Madero-Pérez J, Fernández B, Lara Ordóñez AJ, Fdez E, Lobbestael E, Baekelandt V, Hilfiker S. RAB7L1-Mediated Relocalization of LRRK2 to the Golgi Complex Causes Centrosomal Deficits via RAB8A. Front Mol Neurosci. 2018 Nov 13;11:417.

McGrath E, Waschbüsch D, Baker BM, Khan AR. LRRK2 binds to the Rab32 subfamily in a GTP-dependent manner via its armadillo domain. Small GTPases. 2021 Mar;12(2):133-146.

McQuin C, Goodman A, Chernyshev V, Kamentsky L, Cimini BA, Karhohs KW, Doan M, Ding L, Rafelski SM, Thirstrup D, Wiegraebe W, Singh S, Becker T, Caicedo JC, Carpenter AE (2018). CellProfiler 3.0: Next-generation image processing for biology. PLoS Biol. 16(7):e2005970.

Mirdita, M., Schütze, K., Moriwaki, Y. *et al.* ColabFold: making protein folding accessible to all. *Nat Methods* **19**, 679–682 (2022).

Myasnikov A, Zhu H, Hixson P, Xie B, Yu K, Pitre A, Peng J, Sun J. Structural analysis of the full-length human LRRK2. Cell. 2021 Jun 24;184(13):3519-3527.e10.

Nichols WC, Elsaesser VE, Pankratz N, Pauciulo MW, Marek DK, Halter CA, Rudolph A, Shults CW, Foroud T; Parkinson Study Group-PROGENI Investigators. LRRK2 mutation analysis in Parkinson disease families with evidence of linkage to PARK8. Neurology. 2007 Oct 30;69(18):1737-44.

Pettersen EF, Goddard TD, Huang CC, Couch GS, Greenblatt DM, Meng EC, Ferrin TE. UCSF Chimera--a visualization system for exploratory research and analysis. *J Comput Chem.* 2004 Oct;25(13):1605-12.

Pfeffer SR. Rab GTPases: master regulators that establish the secretory and endocytic pathways. Mol Biol Cell. 2017 Mar 15;28(6):712-715.

Purlyte E, Dhekne HS, Sarhan AR, et al. Rab29 activation of the Parkinson's disease-associated LRRK2 kinase. Embo J. 2018;37:1–18.

791 Purlyte E, Kalogeropulou A, Tonelli F, Alessi DR 2022. Immunofluorescence-based assay to
792 assess LRRK2 association with microtubules in HEK293 cells. **Protocols.io**
793 https://dx.doi.org/10.17504/protocols.io.b5jhq4j6

794 R Core Team (2021). R: A language and environment for statistical computing. R Foundation for
795 Statistical Computing, Vienna, Austria https://www.R-project.org/.

796 Schapansky J, Nardozzi JD, Felizia F, LaVoie MJ. Membrane recruitment of endogenous
797 LRRK2 precedes its potent regulation of autophagy. Hum Mol Genet. 2014 Aug 15;23(16):4201-
798 14.

799 Seaman MN (2004) Cargo-selective endosomal sorting for retrieval to the Golgi requires
800 retromer. J Cell Biol 165: 111–122

801 Sen S, Webber PJ, West AB (2009) Dependence of leucine-rich repeat kinase 2 (LRRK2)
802 kinase activity on dimerization. J Biol Chem 284(52):36346–36356.

803 Sobu Y, Wawro PS, Dhekne HS, Yeshaw WM, Pfeffer SR. Pathogenic LRRK2 regulates
804 ciliation probability upstream of tau tubulin kinase 2 via Rab10 and RILPL1 proteins. Proc Natl
805 Acad Sci U S A. 2021 Mar 9;118(10):e2005894118.

806 Sönnichsen B, De Renzis S, Nielsen E, Rietdorf J, Zerial M. Distinct membrane domains on
807 endosomes in the recycling pathway visualized by multicolor imaging of Rab4, Rab5, and
808 Rab11. J Cell Biol. 2000 May 15;149(4):901-14.

809 Steger M, Diez F, Dhekne HS, Lis P, Nirujogi RS, Karayel O, Tonelli F, Martinez TN, Lorentzen
810 E, Pfeffer SR, Alessi DR, Mann M. Systematic proteomic analysis of LRRK2-mediated Rab
811 GTPase phosphorylation establishes a connection to ciliogenesis. Elife. 2017 Nov 10;6:e31012.

812 Steger M, Tonelli F, Ito G, Davies P, Trost M, Vetter M, Wachter S, Lorentzen E, Duddy G,
813 Wilson S, Baptista MA, Fiske BK, Fell MJ, Morrow JA, Reith AD, Alessi DR, Mann M.
814 Phosphoproteomics reveals that Parkinson's disease kinase LRRK2 regulates a subset of Rab
815 GTPases. Elife. 2016 Jan 29;5:e12813.

816 Stirling DR, Swain-Bowden MJ, Lucas AM, Carpenter AE, Cimini BA, Goodman A (2021).
817 CellProfiler 4: improvements in speed, utility and usability. BMC Bioinformatics, 22 (1), 433.

818 Tasegian A, Singh F, Ganley IG, Reith AD, Alessi DR. Impact of Type II LRRK2 inhibitors on
819 signaling and mitophagy. Biochem J. 2021 Oct 15;478(19):3555-3573.

820 Thomas LL, Fromme JC. 2016. GTPase cross talk regulates TRAPPII activation of Rab11
821 homologues during vesicle biogenesis. J Cell Biol. 215(4):499-513.

822 Tonelli, F and Alessi D. 2021. Quantitative Immunoblotting Analysis of LRRK2 Signalling
823 Pathway. **Protocols.io** https://dx.doi.org/10.17504/protocols.io.bsgrnbv6

824 Vides EG, Pfeffer SR 2021. Microscale Thermophoresis determination of Rab29 binding to
825 LRRK2 Armadillo Domain. Protocols.io https://dx.doi.org/10.17504/protocols.io.bvvmn646

826 Viewegg S, Mulholland K, Brauning B, Kachariya N, Lai Y, Toth R, Kishor Singh R, Volpi I,
827 Sattler M, Groll M, Itzen A, Muqit MMK. PINK1-dependent phosphorylation of Serine111 within
828 the SF3 motif of Rab GTPases impairs effector interactions and LRRK2-mediated
829 phosphorylation at Threonine72. Biochem J. 2020 May 15; 477(9):1651-1668.

830 Waschbüsch D, Michels H, Strassheim S, Ossendorf E, Kessler D, Gloeckner CJ, et al. (2014)
831 LRRK2 Transport Is Regulated by Its Novel Interacting Partner Rab32. PLoS ONE 9(10):
832 e111632.

833 Waschbüsch D, Purlyte E, Pal P, McGrath E, Alessi DR, Khan AR (2020) Structural Basis for
834 Rab8a Recruitment of RILPL2 via LRRK2 Phosphorylation of Switch 2. Structure 28, 406-417.

835 Zhu H, Tonelli F, Alessi DR, Sun J (2022) Structural basis of human LRRK2 membrane
836 recruitment and activation. bioRxiv 2022.04.26.489605; doi:
837 https://doi.org/10.1101/2022.04.26.489605

838

839 **Figure Legends**

840 **Figure 1.** Rab29 binds to the C-terminal portion of the LRRK2 Armadillo domain.
841 Microscale thermophoresis of full length (residues 1-552), labeled LRRK2 Armadillo
842 domain with His-Rab29 (A) or with His-Rab7 (B). (C, D) Microscale thermophoresis of
843 labeled LRRK2 Armadillo domain residues 1-159 (C) or 350-550 (D) with Rab29.
844 Purified Rab29 was serially diluted and then NHS-RED labeled-LRRK2 Armadillo (final
845 concentration 100nM) was added. Graphs show mean and SEM from three
846 independent measurements, each from a different set of protein preparations.

847 **Figure 2.** Rab8A and Rab10 bind to the LRRK2 Armadillo domain. (A-C) Microscale
848 thermophoresis of labeled, LRRK2 Armadillo domain fragments comprised of residues
849 1-552, 1-159, or 350-550 with Rab8A Q67L (1-181) as indicated. (C, D, E) Microscale
850 thermophoresis for Rab10 Q68L (1-181) with indicated LRRK2 Armadillo fragments, as
851 in A. Purified Rab proteins were serially diluted and then NHS-RED labeled LRRK2
852 Armadillo domain (final concentration 100nM) was added. Graphs show mean and SEM

853 from three independent measurements, each from a different set of protein
854 preparations.

855 **Figure 3.** Characterization of critical LRRK2 residues mediating binding to Rab29. (A)
856 Predicted interactions between Rab29 and the LRRK2 Armadillo domain using
857 AlphaFold docking (Jumper et al., 2021), ColabFold (Mirdita et al., 2021) and the
858 AlphaFold2_advanced.ipynb notebook default settings. Residues identified in red show
859 key contacts between LRRK2 and Rab29; orange and yellow coloring indicates the
860 Switch I and Switch II domains of Rab29. (B) The wild type and indicated mutants of full
861 length of GFP-LRRK2 were co-expressed with HA-Rab29 in HeLa cells. 24h post
862 transfection cells were fixed and localization assessed by confocal microscopy. LRRK2
863 overlap with Rab29 is presented as a Mander's coefficient determined using Cellprofiler
864 software (McQuin et al., 2018). (C, D) Wild type and indicated mutants of full length of
865 GFP-LRRK2 (C) or GFP-LRRK2 R1441G (D) were co-expressed with HA-Rab29 in
866 HEK293T cells. 24h post transfection, cells were lysed and extracts immunoblotted with
867 the indicated antibodies. Shown are the averages and standard deviations of duplicate
868 determinations; red asterisks indicate preferred mutant.

869 **Figure 3 - Figure Supplement 1.** (top) Fragments of GFP-LRRK2 that were co-
870 expressed with HA-Rab29 in HeLa cells. 24h post transfection, cells were fixed and
871 localization assessed by confocal microscopy. Fragments that co-localized with Rab29
872 at the Golgi are shown in green and those that failed to co-localize in gray. The
873 smallest fragment of LRRK2 that co-localized with Rab29 encompassed residues 350-
874 550 (shown below). Magnification bar, 20μm.

875 **Figure 3 - Figure Supplement 2.** (A) Alphafold model of a complex of Rab29 (grey)
876 bound to the 350-550 fragment of LRRK2 (purple) as in Fig. 3A. (B) Table of Site #1
877 residues predicted to lie within the interface of LRRK2 and Rab29. Highlighted in red
878 are residues that when mutated, suppress interaction of LRRK2 with Rab29 and inhibit
879 Rab29-mediated LRRK2 activation in cells. (C) Alphafold model of a complex of Rab8A
880 (grey) bound to the 350-550 fragment of LRRK2 (navy); red residues are R361, R399,
881 L403 and K439.

882 **Figure 3 - Figure Supplement 3.** Examples of micrographs used to create Fig. 3B.
883 Mutants (indicated) of full length GFP-LRRK2 were co-expressed with HA-Rab29 in
884 HeLa cells. 24h post transfection, cells were fixed and localization assessed by confocal
885 microscopy. Magnification bar, 20μm.

886 **Figure 3 - Figure Supplement 4.** Immunoblots used to obtain Fig. 3C and Fig. 3D.
887 Wild type and indicated mutants of full length of GFP-LRRK2 (A) or R1441G LRRK2 (B)
888 were co-expressed with HA-Rab29 in HEK293T cells. 24h post transfection cells were
889 fixed and samples analyzed for immunoblotting. Each membrane was probed with anti-
890 pRab10 (rabbit), anti-Rab10 (mouse) and anti-HA (rat) antibodies. pRab10 and Rab10
891 signals were detected using 800 (anti-rabbit) and 680 (anti-mouse) channels in LICOR,
892 whereas the HA (showing Rab29 expression) was developed using ECL (anti-rat).

893 **Figure 4.** phosphoRab8A and phosphoRab10 bind with high affinity to the N-terminal
894 portion of the LRRK2 Armadillo domain. (A-F) Microscale thermophoresis of labeled,
895 indicated, LRRK2 Armadillo fragments with His-phosphoRab8A Q67L 1-181 (A-C) or
896 with His phosphoRab10 Q68L 1-181 (pRab10 (D-F). Purified Rab proteins were
897 phosphorylated with Mst3 kinase at 27°C for 2 h and then serially diluted; NHS-RED

898 labeled Armadillo (final concentration 100 nM) was then added. Graphs show mean and
899 SEM from three independent measurements, each from a different set of protein
900 preparations.

901

902 **Figure 5.** A. Electrostatic surface potential of LRRK2 Armadillo domain residues 1-552
903 modeled using Chimera 2 software (Petterson et al., 2004); blue indicates a positively
904 charged surface. LRRK2 K17 and K18 are indicated. (B) Alphafold (Jumper et al.,
905 2021) structure of putative, active LRRK2 with residues that mediate Rab29 binding
906 shown in red (Site #1) and the K17/K18 residues that are required for phosphoRab10
907 binding (Site #2) shown in magenta; the kinase domain is shown in blue. (C,D)
908 Microscale thermophoresis of labeled, full length LRRK2 K17A or K18A Armadillo 1-552
909 with His phosphoRab10 Q68L 1-181. Purified Rab10 protein was phosphorylated with
910 Mst3 kinase at 27°C for 2 h and then serially diluted; NHS-RED labeled Armadillo (final
911 concentration 100 nM) was then added. Graphs show mean and SEM from three
912 independent measurements, each from a different set of protein preparations.

913 **Figure 6.** LRRK2 K17 and K18 are critical for pRab10 interactions in cells. (A) FLAG-
914 LRRK2 R1441G (red) was transfected into HeLa cells plated on collagen coated
915 coverslips and co-localized with endogenous wild type pRab10 (green). Cells on
916 coverslips were dipped in liquid nitrogen to deplete cytosol and enhance membrane-
917 bound signal. Insets show enlargements of boxed areas representing peri-centriolar
918 LRRK2 and pRab10. (B) FLAG-LRRK2 R1441G/K17A/K18A (red) was transfected into
919 HeLa cells plated on collagen coated coverslips and stained and localized with pRab10

920 (green) as in A. (C) Quantification of pRab10 overlap with LRRK2 by Mander's
921 coefficient. Error bars represent SEM of means from three different experiments
922 (represented by colored dots), each with >40 cells per condition. Significance was
923 determined by *t* test, *P = 0.0108.

924 **Figure 7**. LRRK2 K17 and K18 increase endogenous pRab10 recovery after LRRK2
925 inhibitor washout. (A-D) FLAG-LRRK2 R1441G, FLAG-LRRK2 R1441G/K17A/K18A,
926 LRRK2, or LRRK2 K17A/K18A was transfected into HeLa cells. 48 hr post transfection
927 cells were treated with 200nM of MLi-2 for 1 hr. The MLi-2 was then removed by
928 multiple washes and incubated for the indicated times prior to cell lysis. Whole cell
929 extracts (20µg) were subjected to quantitative immunoblot analysis using anti-LRRK2,
930 anti-Rab10, and anti-pRab10 antibodies. (E-F) Quantification of pRab10/ total Rab10
931 fold change and normalized to no MLi2 control. Error bars represent mean ± SD from 2
932 different experiments per condition.

933 **Figure 8.** Feed-forward pathway for Rab10 phosphorylation is dependent on LRRK2
934 kinase activity. (A) Fluorescence intensity traces of individual, single molecules of 7nM
935 CF633-labeled FLAG-LRRK2 R1441G on a substrate supported lipid bilayer decorated
936 with lipid anchored GFP-Rab10 Q68L-His across 600 sec of live TIRF microscopy.
937 Red, R1441G; Blue, K17A/K18A/R1441G; Yellow, D2017A. B. Reactions were carried
938 out as in (A) except Rab10 was omitted (purple) or Rab10 was replaced with Rab11
939 (green). Dashed lines in A and B represent time of addition of fluorescently labeled
940 LRRK2 at 60 sec. Fluorescence intensity was fitted by a nonlinear regression curve for
941 two phase association. Fold change was calculated by dividing the average
942 fluorescence intensity at steady state and subtracting background fluorescence intensity

943 average determined from 60 sec prior to LRRK2 addition. C. Rate of membrane
944 association of LRRK2 as a function of Rab10 concentration. This curve was fitted by a
945 nonlinear regression fit using PRISM software (Mathworks) to determine a Hill
946 coefficient.

947 **Figure 8 – Figure Supplement 1.** Quantitative analysis of TIRF images of LRRK2
948 recruitment on planar lipid bilayers. A. Ridge plot showing the distribution of the
949 fluorescence intensity of CF633-labeled LRRK2 molecules (or complexes) as a function
950 of the time elapsed since the molecule first appeared on the surface. Two replicates of
951 LRRK2 are shown. For each molecule, the fluorescence intensity I_t at each time point t
952 was normalized with respect to its initial intensity I_0 during the first frame when the
953 molecule first appeared on the surface. The intensity distributions are shown in log
954 scale (*x* axis). Intensity distributions were computed using the average intensity of each
955 molecule over 25s increments. Purple data points and error bars below each distribution
956 show its mean and standard deviation. For each time point *t*, all the molecules with a
957 fluorescence lifetime greater than *t* were used to compute the distribution. The number
958 of such molecules at each time point is shown in panel E. B. Same ridge plot as in A
959 showing the evolution of the fluorescence intensity with greater temporal resolution
960 during the first 30s after a molecule appeared on the surface. Here, the intensity
961 distributions were computed using the average intensity of each molecule over 1.5s
962 increments. Only molecules with a fluorescence lifetime larger than 30s were included
963 in this ridge plot (N=1171, 2334, and 106 molecules respectively for the 3 conditions
964 shown (left to right). C. Individual fluorescence intensity over time for the 30 molecules

965 with the longest fluorescence lifetimes as in A. D. Ridge plot showing the distribution of
966 the initial fluorescence intensity I_0 of individual CF633-labeled LRRK2 molecules or
967 complexes when they first appeared on the surface, as a function of the time elapsed
968 since the first molecule was detected (referred to as the absolute time *T*). These initial
969 intensities were normalized to the median initial intensity of all molecules. E. Inverse
970 cumulative distribution of the fluorescence lifetime of individual molecules. F.
971 Percentage of molecules that were "ultrabright" when they first appeared on the surface,
972 as a function of the absolute time *T* at which they appeared. Ultrabright refers to
973 molecules with an initial intensity greater than $2^{1.5}$ fold the median initial intensity
974 across all molecules ($\log_2[I_0/\text{median}(I_0)]>1.5$).

975

976 **Figure 8 – Figure Supplement 2.** The LRRK2 Armadillo domain can bind
977 phosphorylated Rab10 and unphosphorylated Rab8A simultaneously. GST-Rab8A was
978 immobilized on glutathione agarose, then LRRK2 Armadillo (or buffer) was added;
979 beads were washed and His-phosphoRab10 Q68L was then added. Bead-bound
980 material (triplicates shown) was eluted with reduced glutathione and analyzed by
981 immunoblotting. Input, 50% of that used in each binding reaction. PhosphoRab10 (5%
982 of input) was detected only in ARM domain-containing samples, consistent with the Kd
983 values.

984

985 **Figure 9.** PhosphoRab8A activates LRRK2 phosphorylation of Rab10 in solution. A.
986 Immunoblot analysis of the kinetics of LRRK2 G2019S phosphorylation of Rab10 with
987 and without additional pRab8. Upper gel, GFP-Rab10 Q68L 1-181 substrate; Lower
988 gel, His-Sumo-Rab10 wild type full length substrate. Indicated reactions contained
989 200nM MLi-2. pRab8A was detected with anti-phosphoRab8A antibody. B. Same as
990 panel A with K18A-LRRK2-R1441G and His-Sumo-Rab10 wild type full length as
991 substrate. PhosphoRab8A was detected with total Rab8 antibody. C. Kinetics of
992 phosphoRab10 production as in A. Shown are the combined means of independent,
993 quadruplicate determinations ± SEM, as indicated. D. PhosphoRab10 production as in
994 B. Shown are the combined means of independent duplicate determinations, ±SEM, as
995 indicated. Background signal in the presence of pRab8A is likely due to trace MST3
996 contamination that is not sensitive to MLi-2 inhibition and was subtracted. pRab8
997 preparation was by Method #1 for A, upper gel, and B, and Method #2 was used in
998 panel A, lower gel.

999 **Figure 10.** A model for LRRK2 membrane recruitment. LRRK2 can interact with non-
1000 phosphorylated Rab GTPases via site #1. Once membrane bound, it can generate
1001 phosphoRabs that can now engage site #2. Rab binding to both sites increases the
1002 avidity of LRRK2 for membranes and retains LRRK2 on the membrane surface to
1003 phosphorylate more Rab substrates. We have shown that LRRK2 binding to
1004 phosphoRabs also activates the kinase, likely by altering its oligomeric state.

1005

1006

1007 **Supporting Videos**

1008 Video 1. TIRF microscopy of R1441G LRRK2 binding to Rab10-lipid bilayers
1009 Captured at 1 frame per second and compressed 20X
1010
1011 Video 2. TIRF microscopy of R1441G LRRK2 binding to lipid bilayers without Rab10
1012 Captured at 1 frame per second and compressed 20X
1013
1014 Video 3. TIRF microscopy of R1441G LRRK2 binding to Rab11-lipid bilayers
1015 Captured at 0.5 frames per second and compressed 40X
1016
1017 Video 4. TIRF microscopy of D2017A LRRK2 binding to Rab10-lipid bilayers
1018 Captured at 1 frame per second and compressed 20X
1019
1020 Video 5. TIRF microscopy of K17A/K18A/R1441G LRRK2 binding to Rab10-lipid bilayers
1021 Captured at 0.5 frames per second and compressed 40X

1022

1023 **Source Data**
1024 Figure 3-figure supplement 4-source data 1. RAW data for gels.
1025 Figure 3-figure supplement 4-source data 2. Annotated gels.
1026
1027 Figure 7-source data 1. RAW data for gels.
1028 Figure 7-source data 2. Annotated gels.
1029
1030 Figure 8-figure supplement 2-source data 1. RAW data for gels.
1031 Figure 8-figure supplement 2-source data 2. Annotated gels.
1032
1033 Figure 9-source data 1. RAW data for gels.
1034 Figure 9-source data 2. Annotated gels.
1035
1036
1037

1038 **Table 1.** Summary of Binding Affinities. Note that these values are likely
1039 underestimates of affinities as typical preparations of purified Rab proteins contained
1040 ~50% bound GDP and ~50% bound GTP by mass spectrometry. Non-phosphorylated
1041 Rab interaction with Armadillo 1-159 is shown in parentheses as it likely reflects binding
1042 to an Alphafold-predicted site near the C-terminus of this fragment that will not be
1043 accessible in full length LRRK2 protein.

1044

	Armadillo 1-159 (Site #2-containing)	Armadillo 1-552	Armadillo 350-550 (Site #1-containing)	Armadillo 1-552 K17A	Armadillo 1-552 K18A
Rab29	>29	1.6 ± 0.9	1.6 ± 0.5	-	-
Rab10-Q68L	(5.1 ± 3.1)	2.4 ± 0.6	5.1 ± 2.5	-	-
pRab10-Q68L	0.71 ± 0.3	1.0 ± 0.4	>29	>20	>20
Rab8A-Q67L	(6.7 ± 3.6)	2.9 ± 1.2	2.3 ± 1.0	-	-
pRab8A-Q67L	1.0 ± 0.6	0.87 ± 0.4	>19.4	-	-
Rab7	-	>6.5	-	-	-

1045

1046

1047

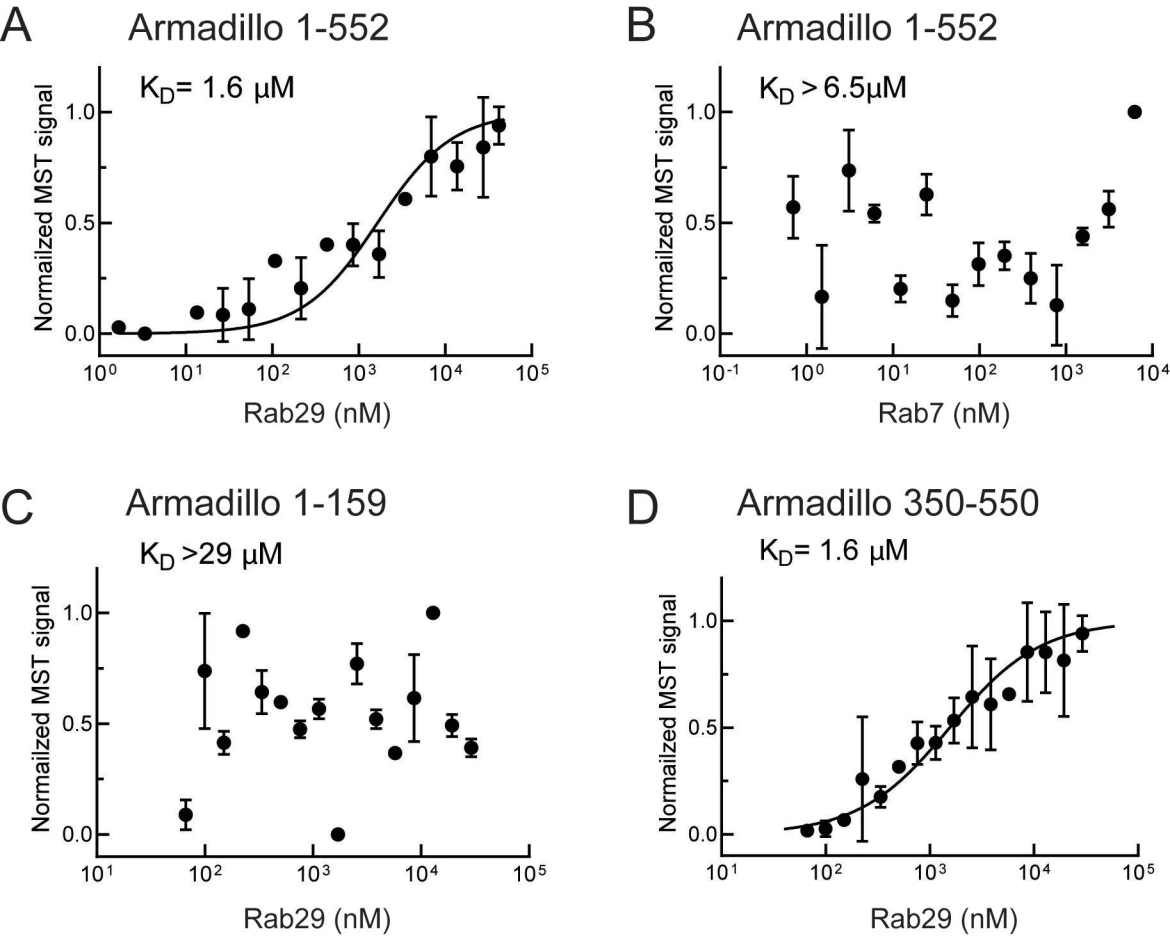

Vides et al., Figure 1

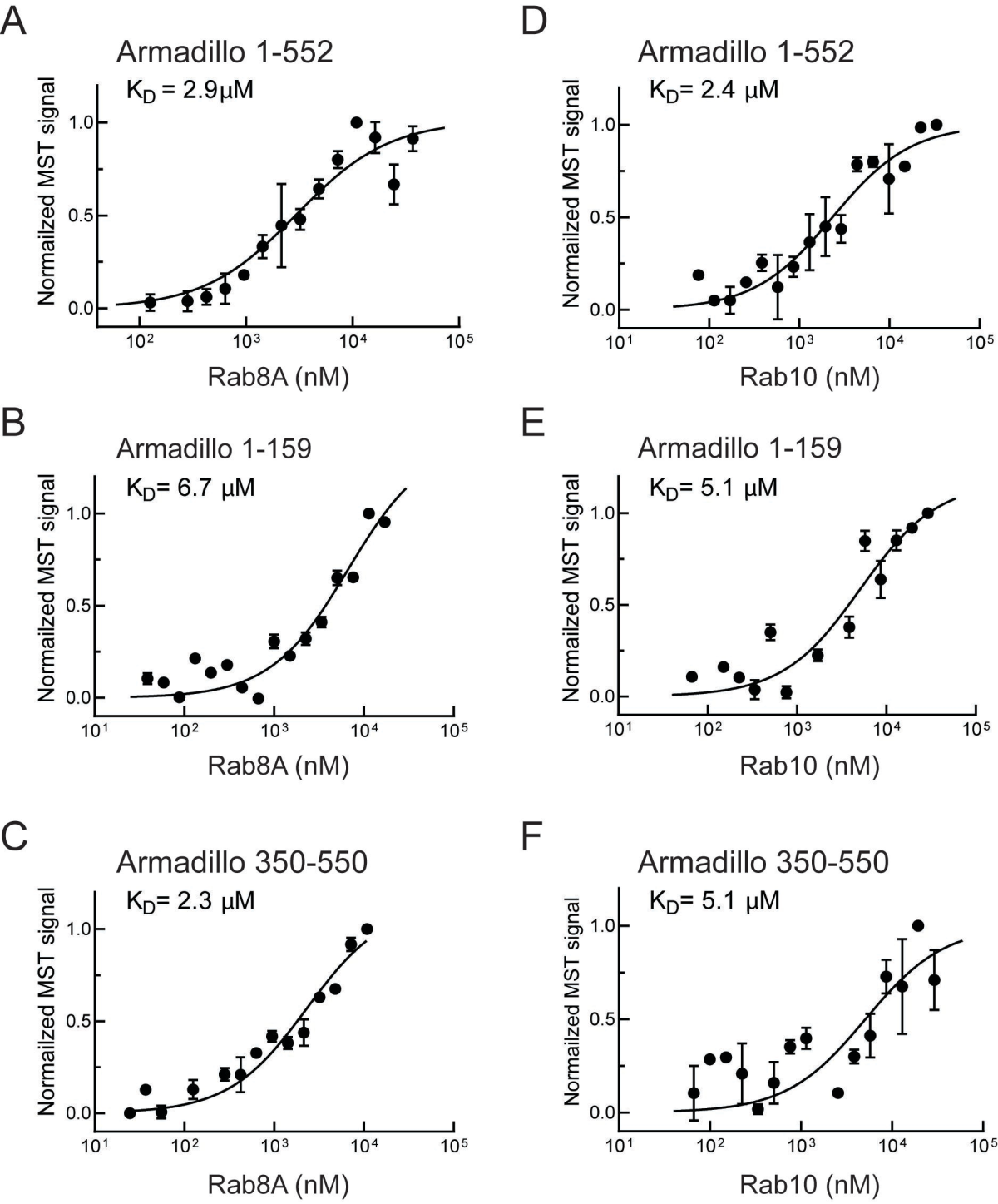

Vides et al., Figure 2

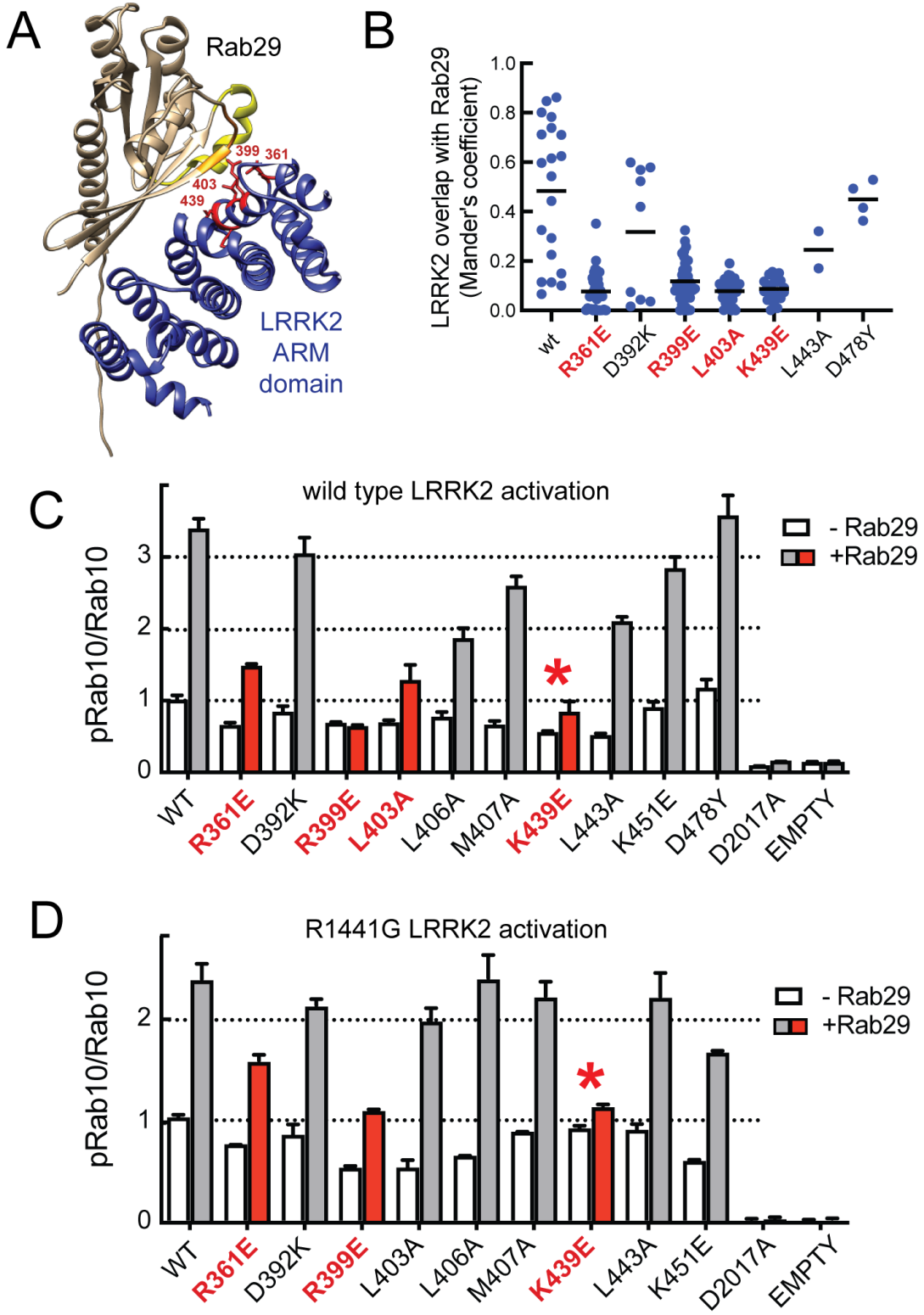

Vides et al., Figure 3

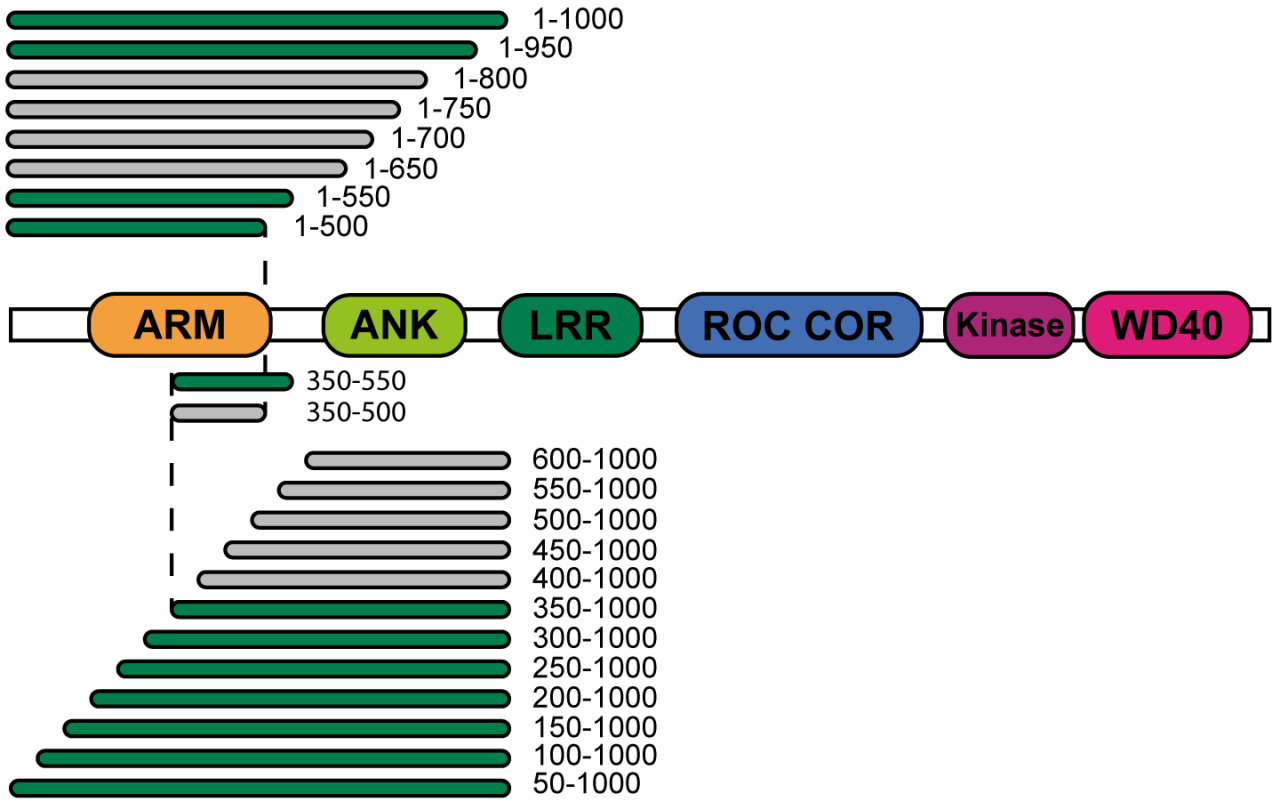

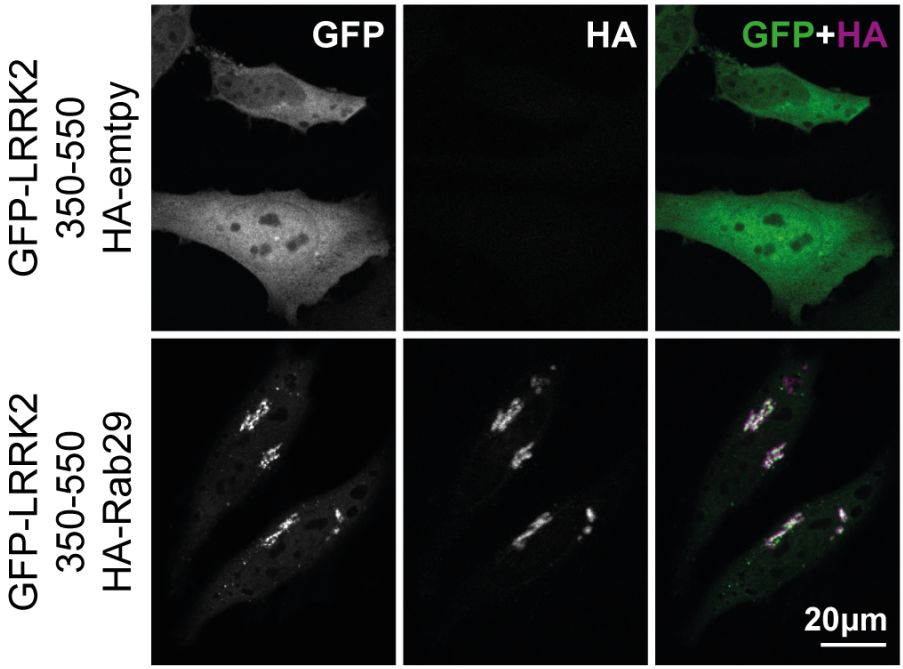

Vides et al. Figure 3 -- Figure Supplement 1

A

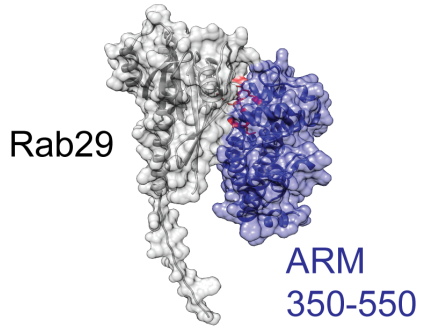

C

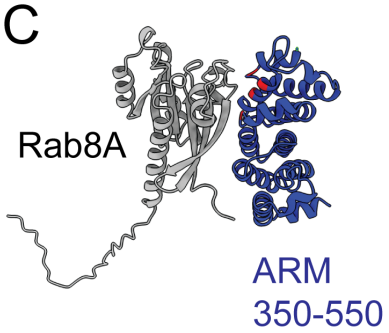

B

LRRK2 (350-550)	Rab29	Distance (Å)	Interaction
R361	Y77	3.07	hydrogen bond
R361	Y77	2.99	hydrogen bond
R361	M73	4.68	hydrophobic
K362	S72	2.48	hydrogen bond
K362	L76	4.44	hydrophobic
D392	K37	3.38	H bond, electrostatic, salt bridge
R399	D43	4.21	electrostatic
L403	V42	5.01	hydrophobic
L406	W62	5.36	hydrophobic
M407	L76	4.99	hydrophobic
M407	Y77	4.73	hydrophobic
K439	D43	3.24	H bond, electrostatic, salt bridge
K439	F44	3.22	hydrogen bond
K439	F44	5.23	hydrophobic
L443	R58	5.30	hydrophobic
K451	D80	4.92	electrostatic

Vides et al., Figure 3 -- Figure Supplement 2

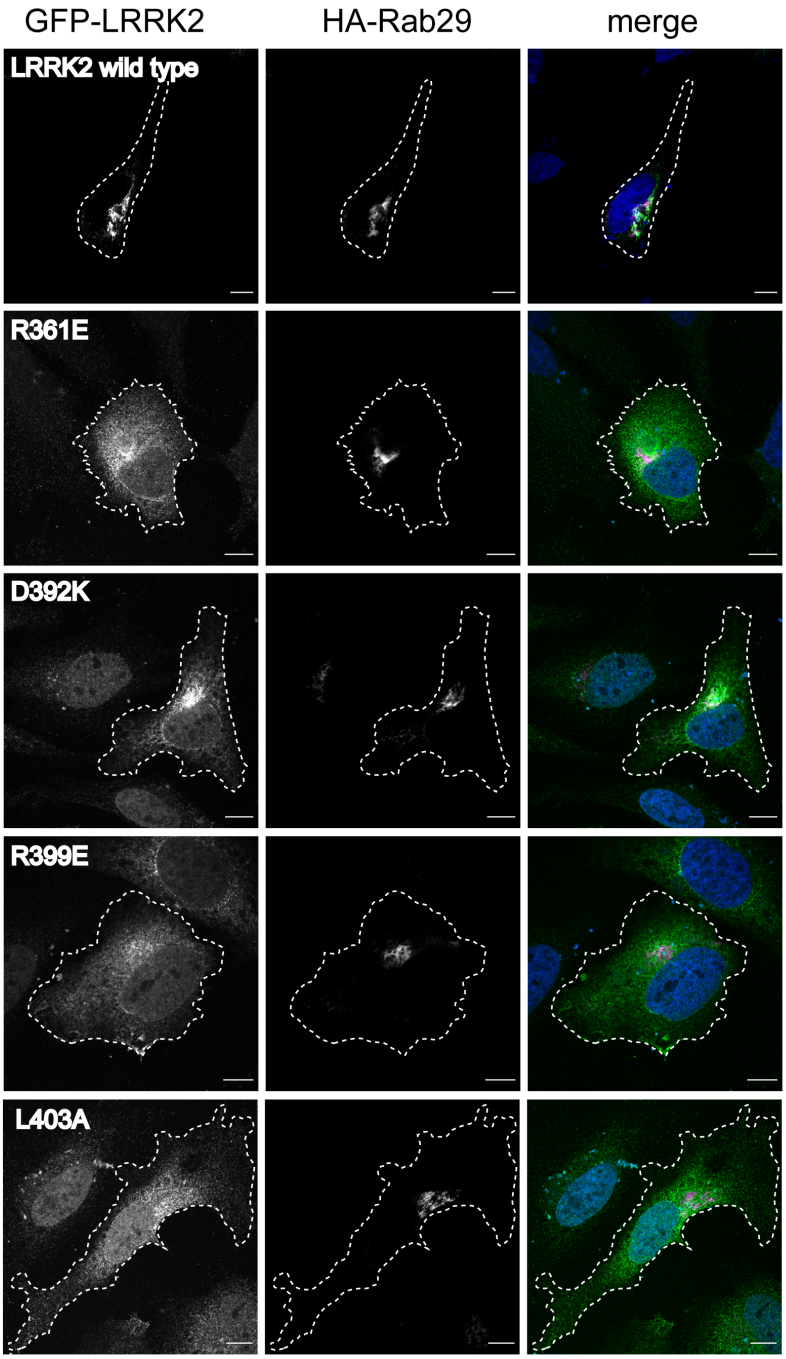

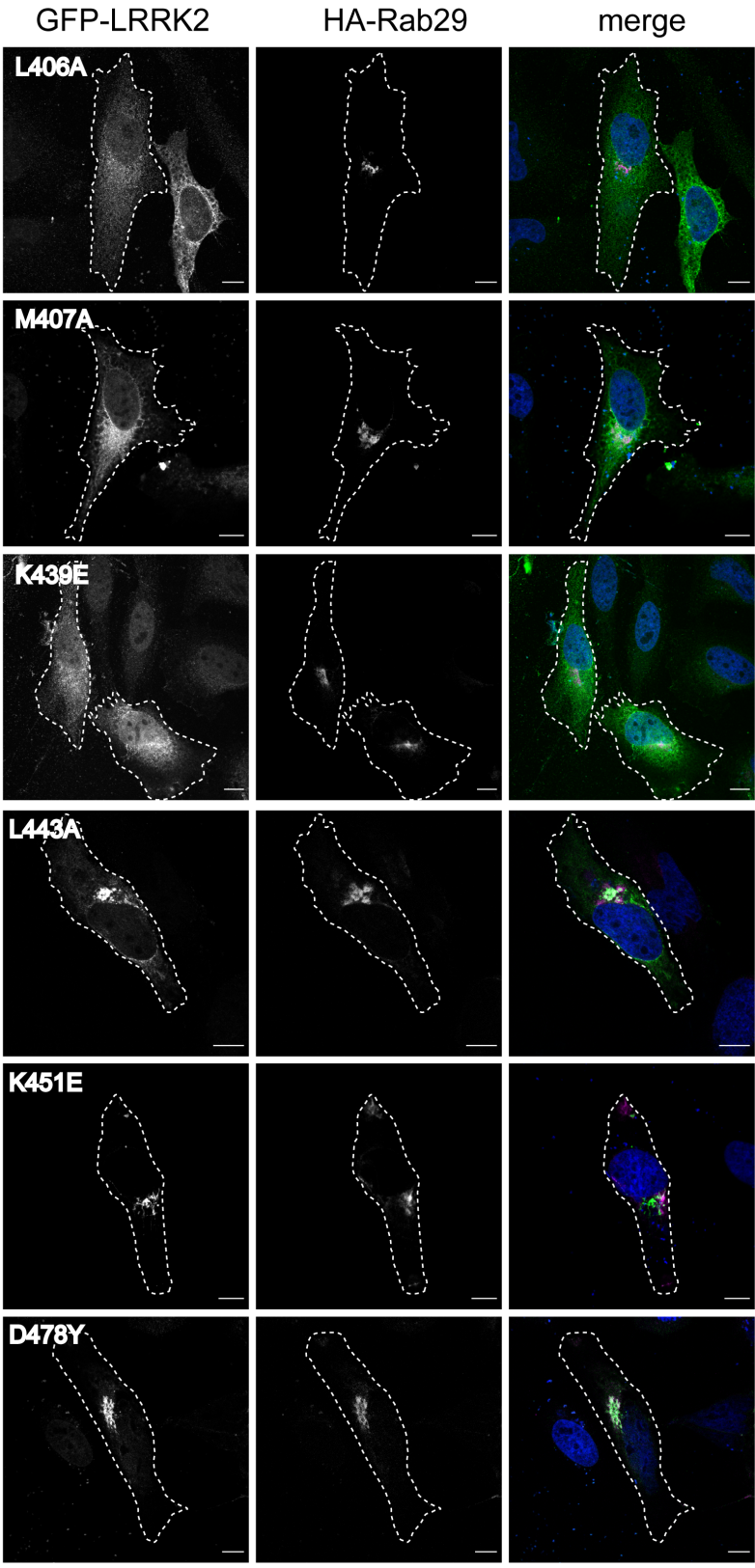

Vides et al., Figure 3 -- Figure Supplement 3

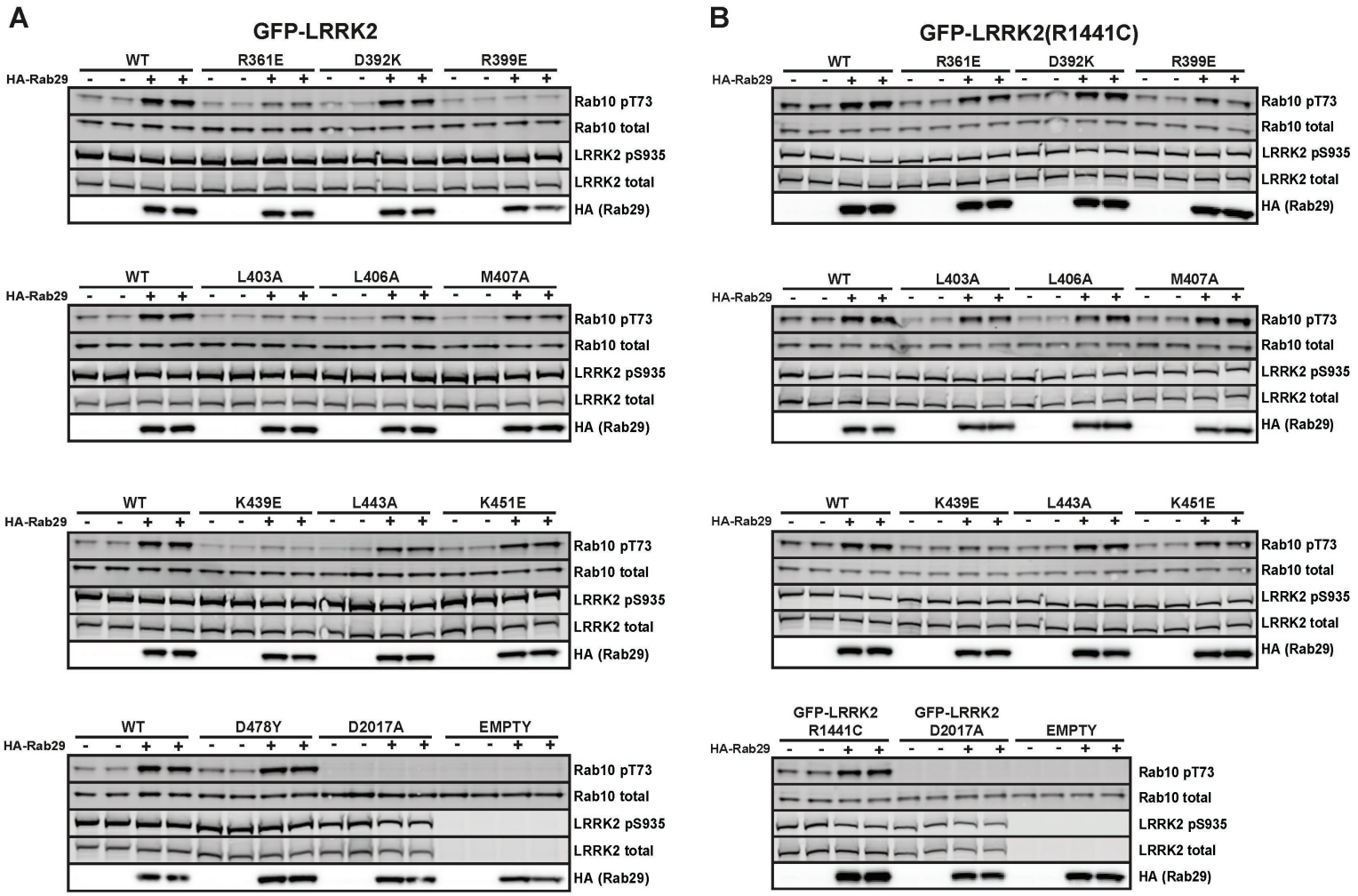

Vides et al. Figure 3--Fig. Supp. 4

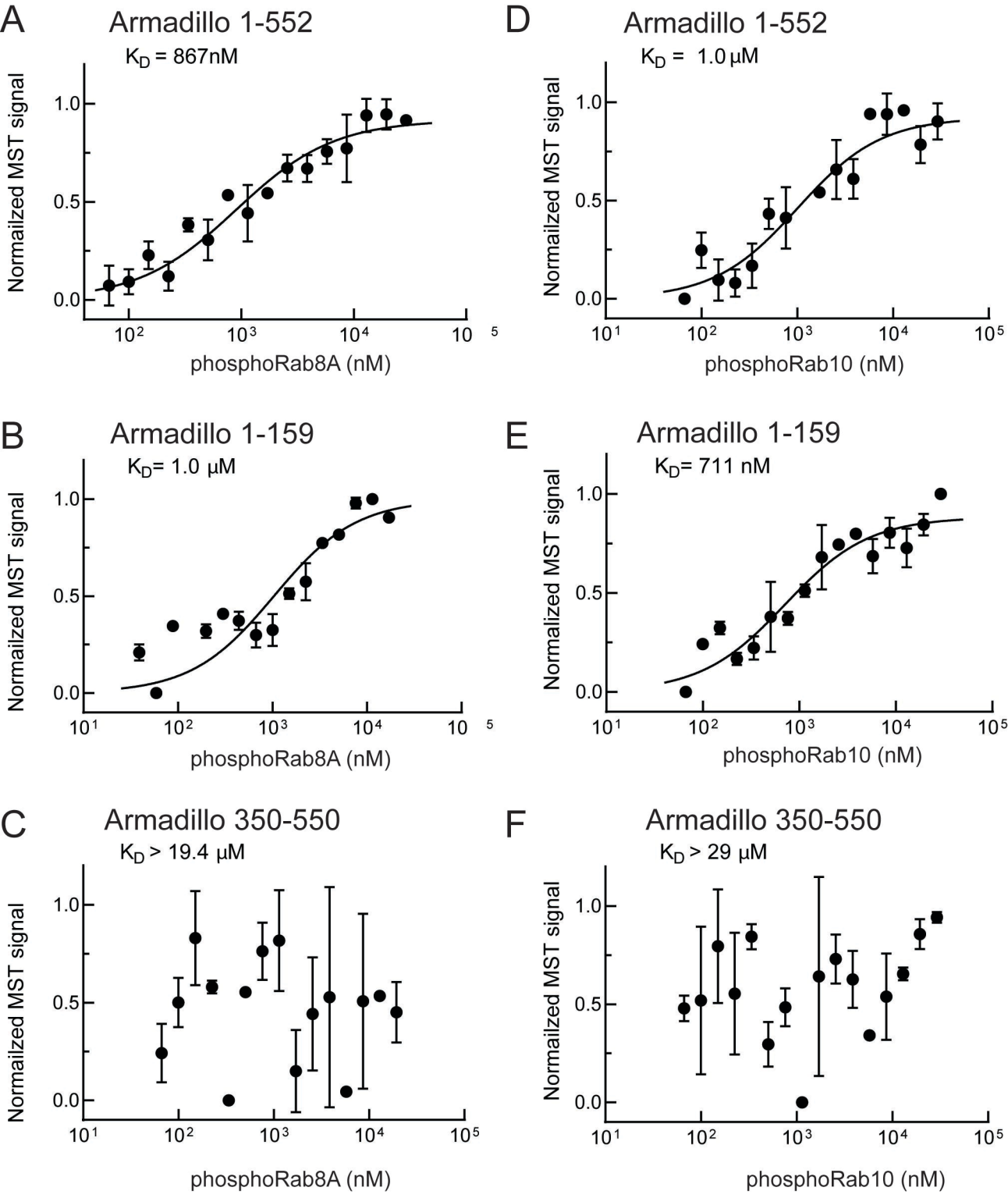

Vides et al., Figure 4

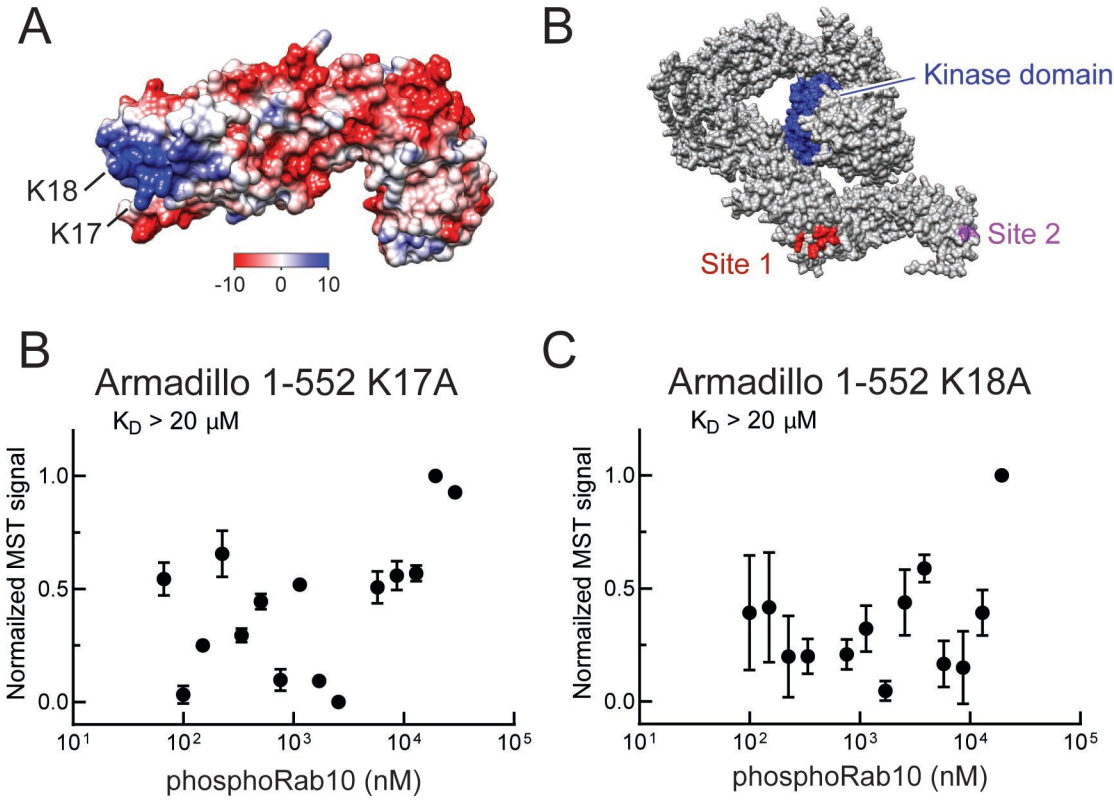

Vides et al., Figure 5

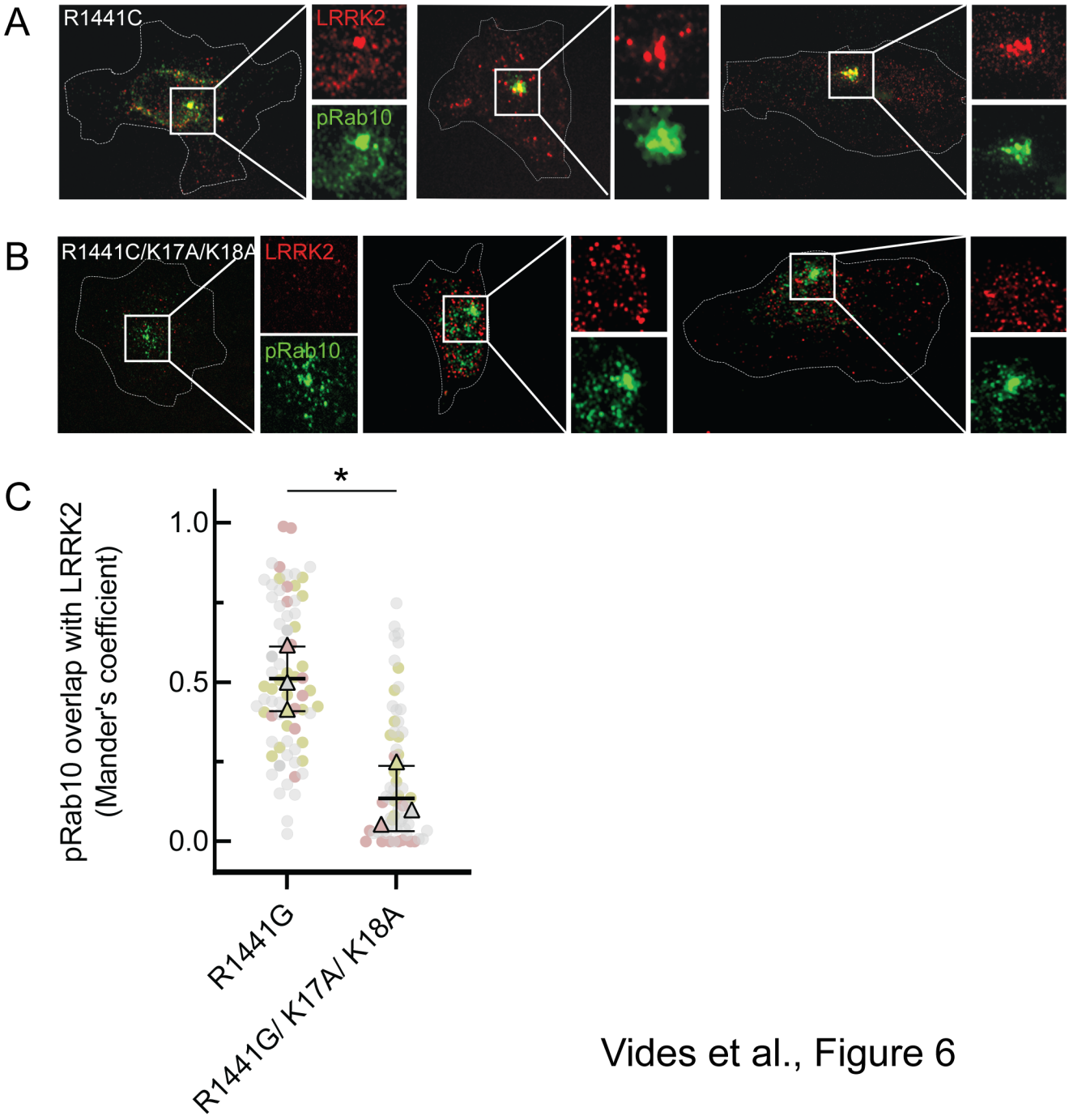

Vides et al., Figure 6

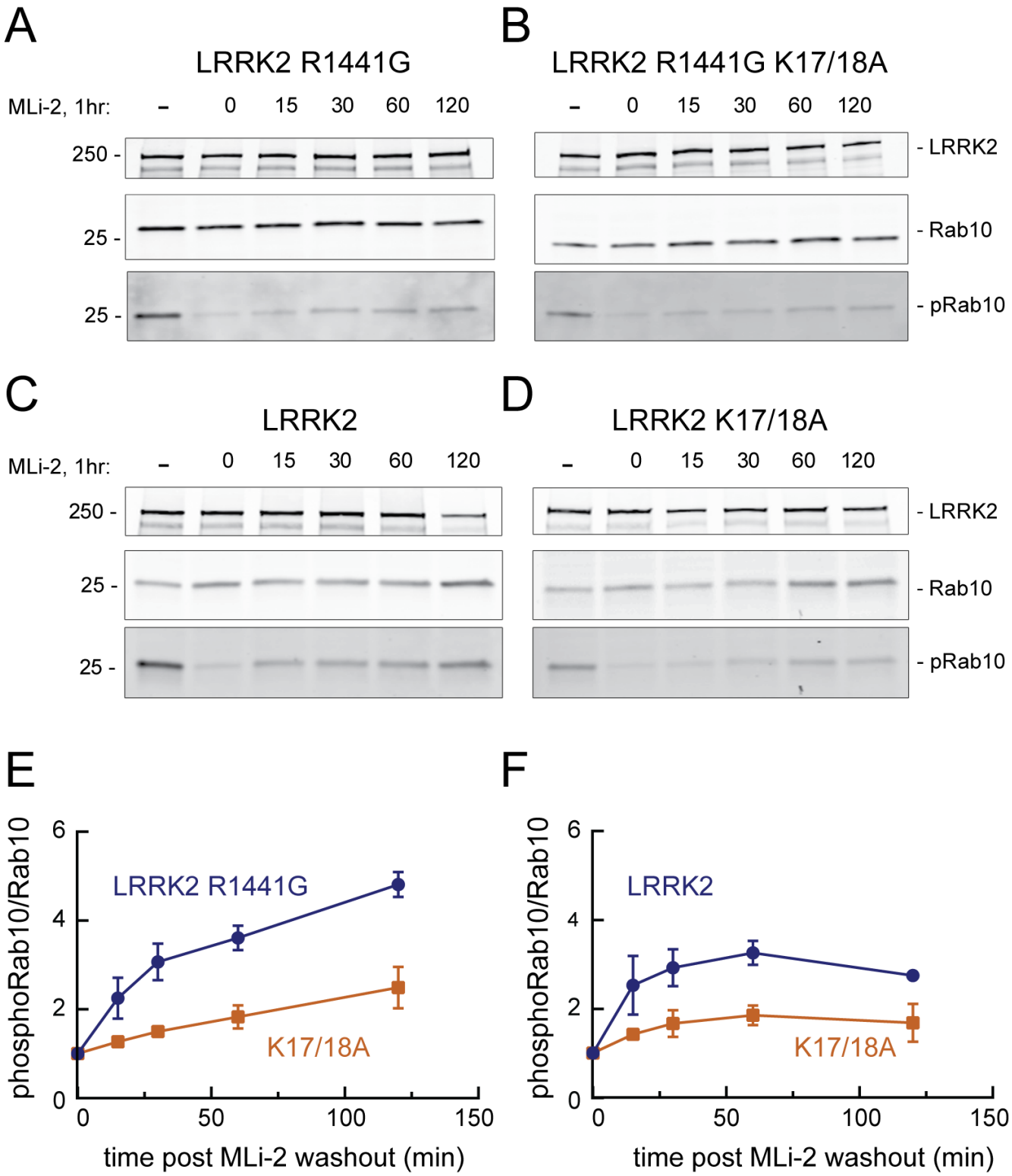

Vides et al., Figure 7

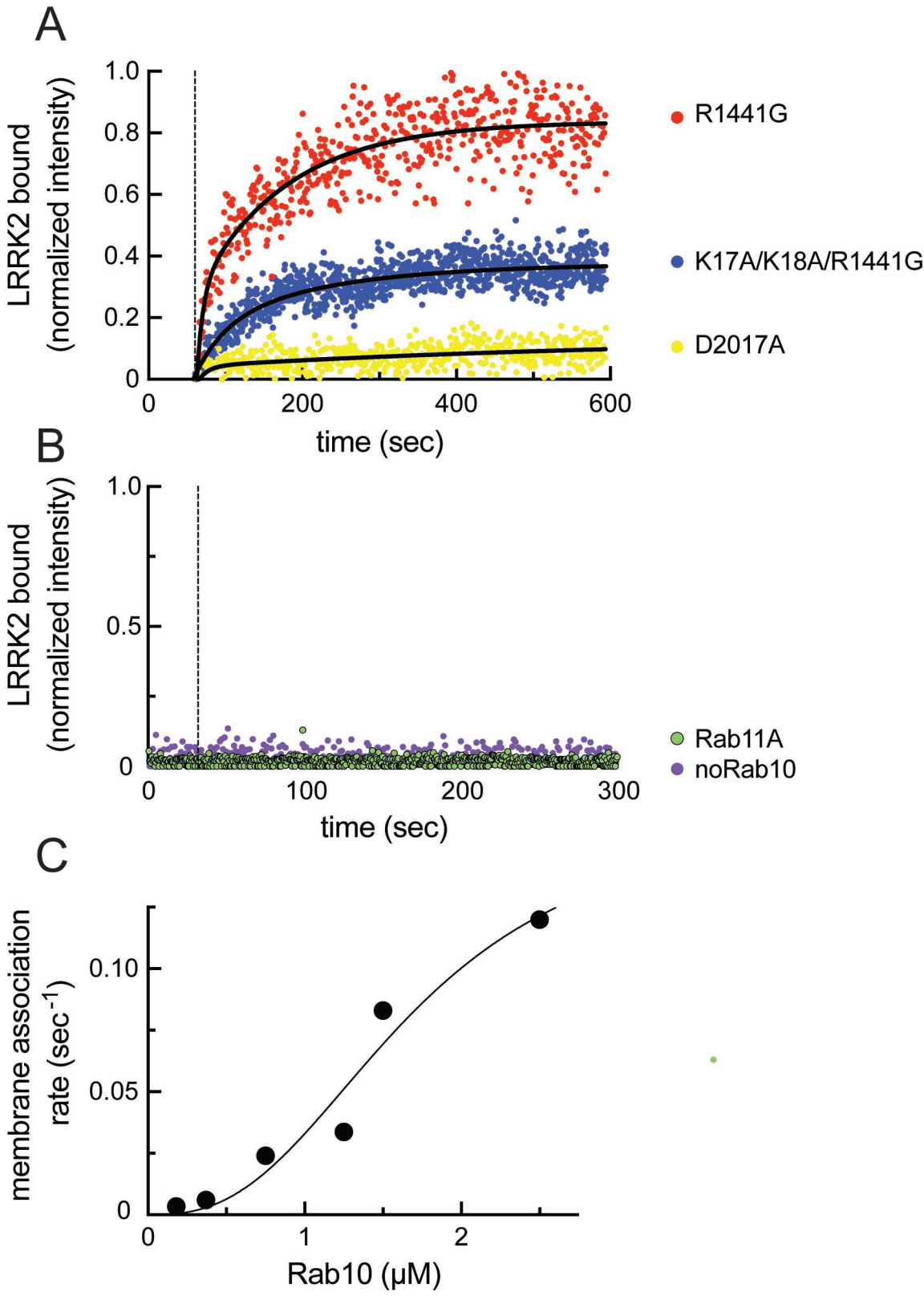

Vides et al., Figure 8

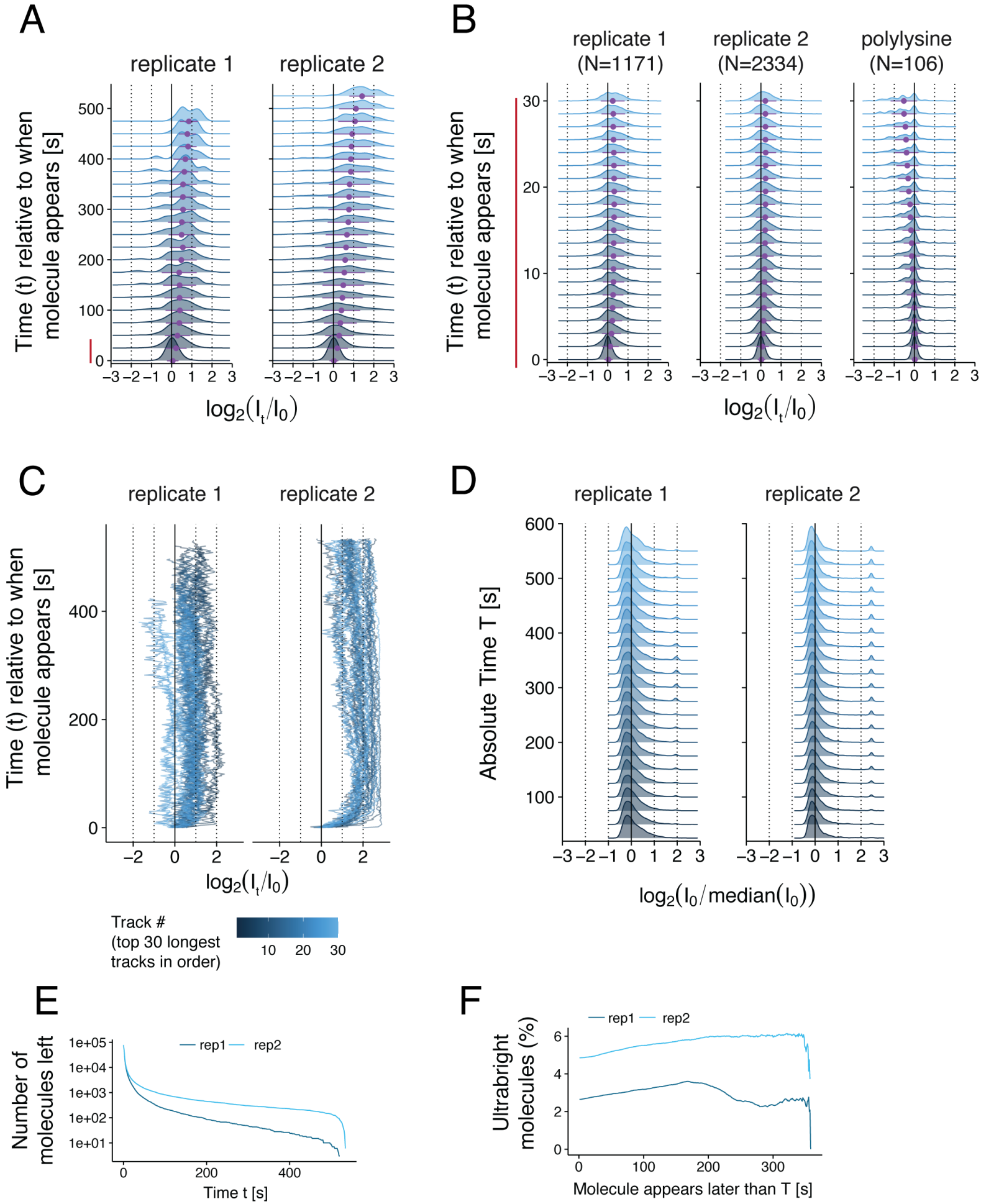

Figure 8 - Figure Supplement 1

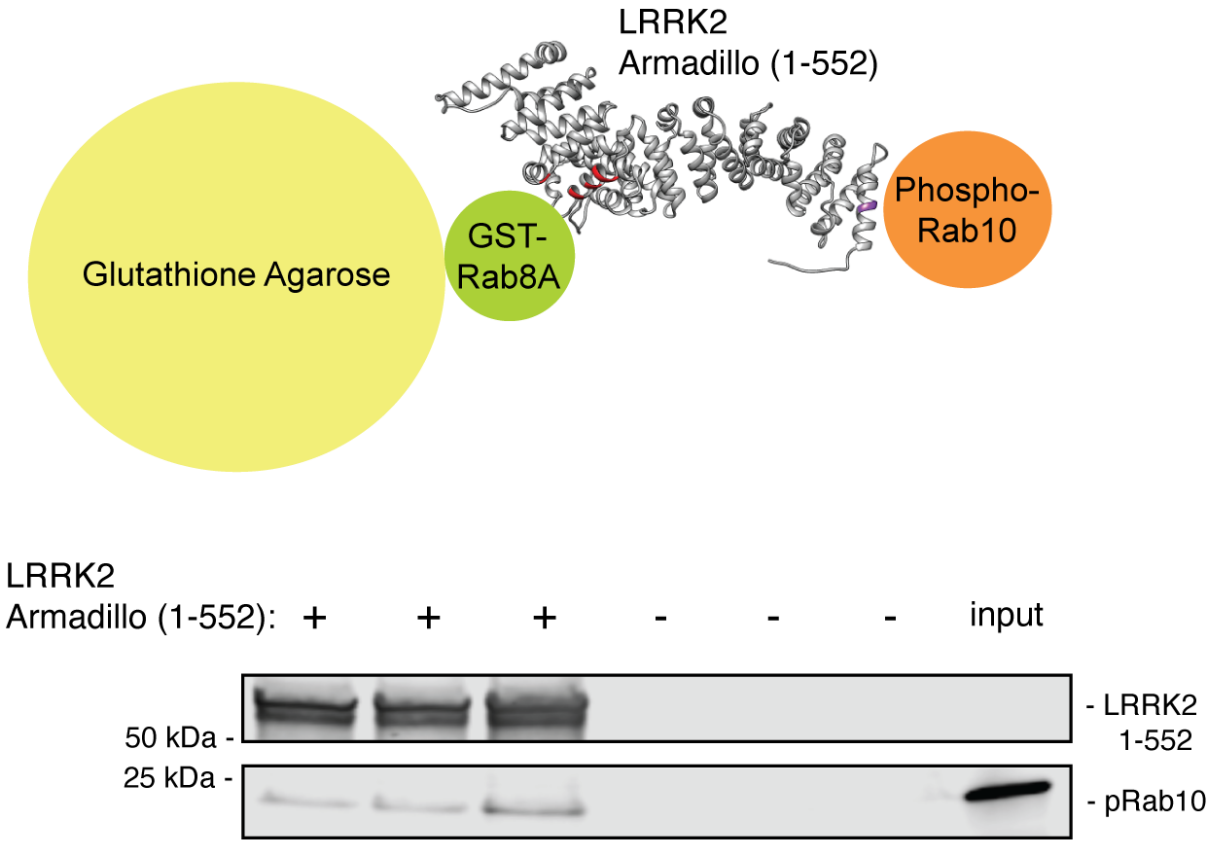

Figure 8 – Figure Supplement 2

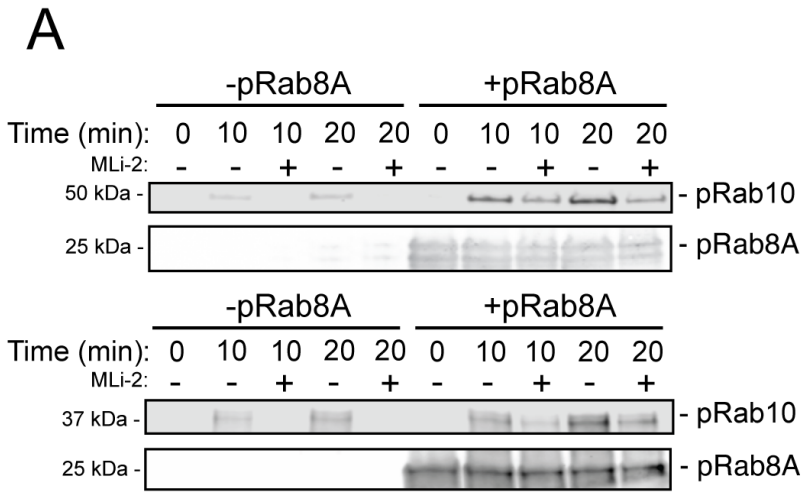

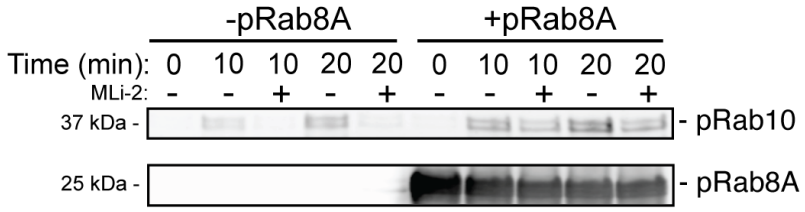

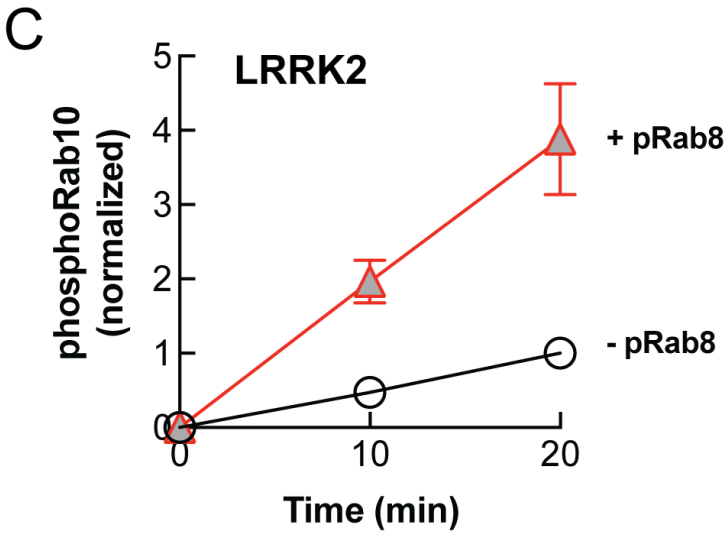

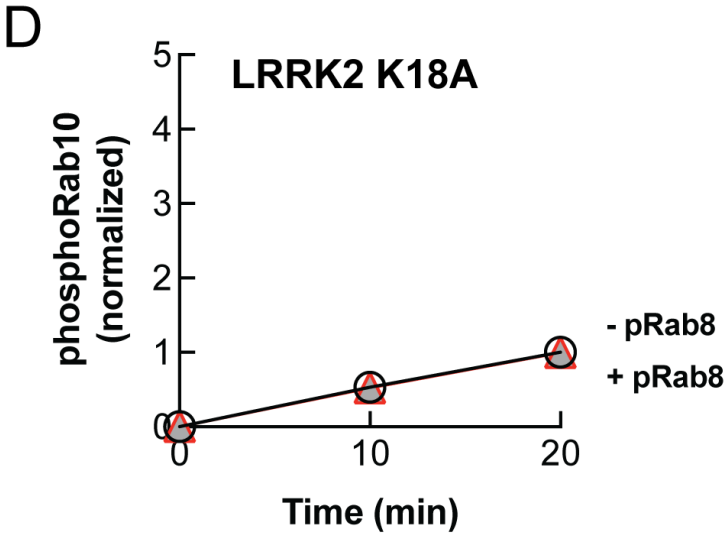

Vides et al., Figure 9

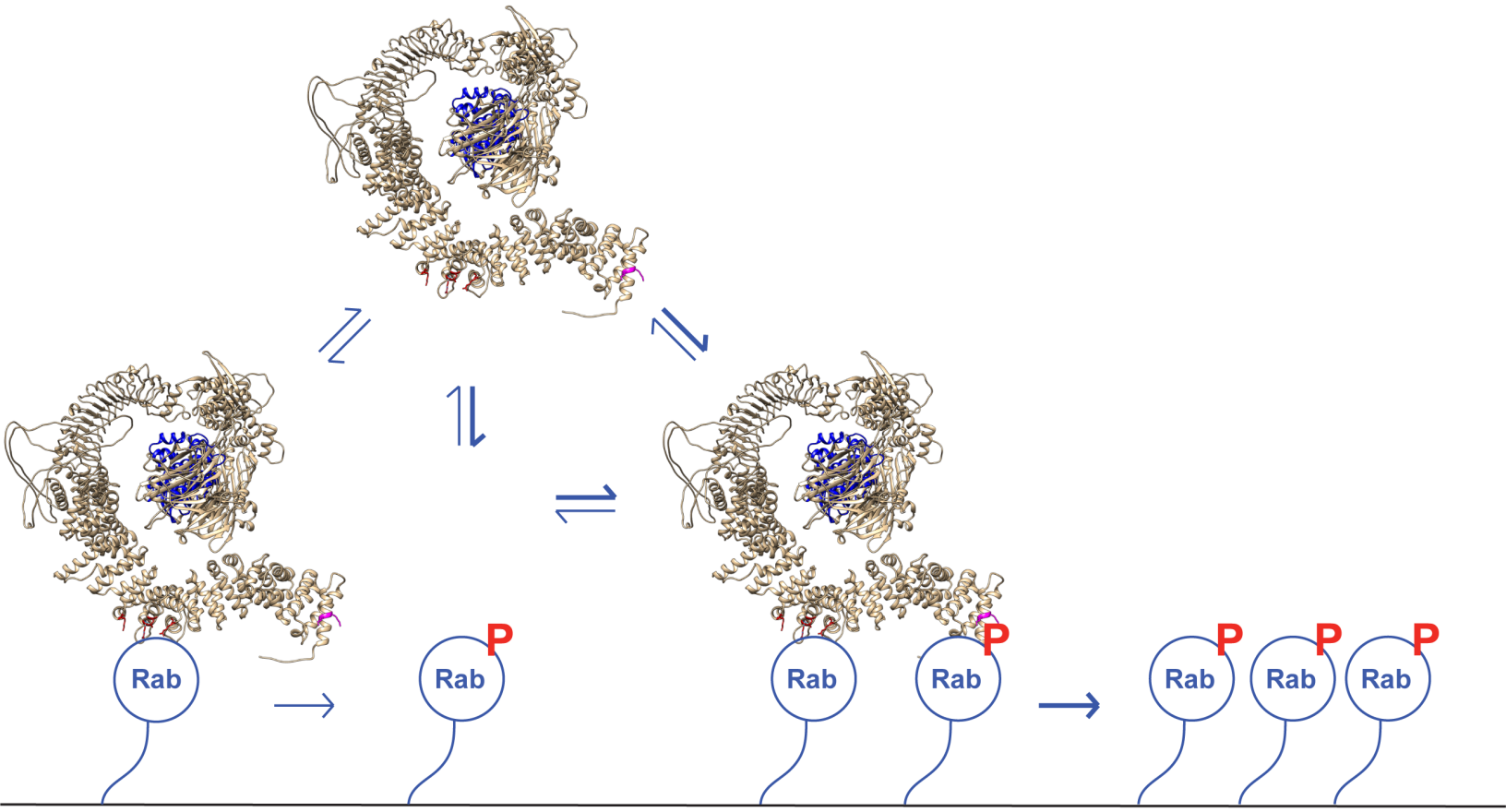

Vides et al., Figure 10